Hybrid Soft-Rigid Elbow Exosuit: Theory, Mechatronic Design, and Experimental Assessment

Ali KhalilianMotamed Bonab, Cristian Camardella, Antonio Frisoli, *Senior Member, IEEE*, and Domenico Chiaradia

***Abstract*—Hybrid wearable robotics, combining soft and rigid elements, offer a promising solution for upper limb assistance by balancing comfort and functionality. This study evaluates a hybrid soft-rigid elbow exosuit designed for elbow movement support in dynamic and endurance tasks, focusing on biomechanical impact, user perception, and ergonomics. A theoretical model guided the design, optimizing device dynamics and assistive force delivery. A generic interaction controller, combined with fixed system parameters, provided effective assistance across participants without the need for subject-specific tuning, simplifying deployment in practical settings. During dynamic tasks, the exosuit significantly reduced biceps muscle activity compared to the unassisted condition, with an average reduction of 28.40% . In endurance tasks, it reduced infraspinatus activity by an average of 44.55% and mitigated increased muscle activation during load-carrying. Subjective assessments indicated lower perceived physical demand, while the system usability scale confirmed high usability and acceptance. These findings highlight the exosuit's ability to reduce physical effort and improve muscle coordination while maintaining comfort. The robust mechatronic design enabled effective assistance through a generic controller, emphasizing the importance of hardware reliability.**

***Index Terms*—Elbow assistance, exosuits, physical human–robot interaction, soft robotics, wearable robot.**

I. Introduction

WEARABLE assistive robotics enhance physical abilities in healthy individuals [1], [2], [3], reduce injury risks [4], [5], and support rehabilitation for limb impairments, aiding recovery, and mobility [1], [3], [6]. While rigid exoskeletons enable precise control and high torque transfer, demonstrating effectiveness in aiding both healthy users and rehabilitation patients [2], [3], [7], their adoption beyond experimental settings remains limited [8]. This is largely due to issues, such as added inertia disrupting natural biomechanics and difficulties in aligning mechanical and biological joints, resulting in bulky designs [8], [9], [10], [11], [12]. The introduction of a new class of assistive robots, known as exosuits, which transmit force and torque to the user through soft materials, has enabled the development of lightweight, compliant, and low-profile devices [13], [14]. These systems rely on the structural integrity of the human body to transfer reaction forces between body segments, rather than using the rigid frame. This approach inherently resolves the issue of misalignment with biological joints and significantly reduces added inertia, thereby minimizing the impact of the device on the user's biomechanics.

Soft robotic wearables have proven effective for both lower and upper limbs. For the lower limbs, they enhance metabolic efficiency and reduce muscle activation during typical movements, such as walking, running, and sitting and standing [15], [16], [17], [18] and support rehabilitation for conditions, such as stroke and Parkinson's disease [19], [20], [21]. Similarly, for the upper limbs, these devices have been effective in assisting workers in industrial settings [22], [23], [24], [25], augmenting human performance [26], and providing therapeutic interventions for conditions including amyotrophic lateral sclerosis, multiple sclerosis, stroke recovery, and tremors [27], [28], [29], [30], [31], [32], [33]. Within soft wearable robotics for the upper limbs, elbow exosuits stand out as promising devices for assisting both non-disabled and impaired individuals. Recent advancements have focused on optimizing their design, actuation, and control for enhanced performance and user comfort [34], [35], [36]. The first cable-driven elbow exosuits were introduced by Koo et al. [37] and Nycz et al. [38]. Masia's group significantly advanced the field, demonstrating reduced muscle activity and delayed fatigue in healthy users [26], [39], [40]. Their device was later tested on chronic stroke [41] and MS patients [29], proving effective in reducing pathological synergies, improving endurance, and enabling physically demanding tasks. Building on the design principles introduced by Xiloyannis [42], several other cable-driven soft elbow exosuit prototypes have been developed [43], [44], [45], [46].

Despite significant advancements in elbow exosuit development, key challenges remain in making these systems practical and robust [6], [35]. Some of these challenges include: improving mechanical and control efficiency and minimizing system nonlinearities; ensuring efficient force transmission through

Received 20 June 2025; revised 25 November 2025; accepted 8 December 2025. Date of publication 14 January 2026; date of current version 5 February 2026. This work was supported in part by the Italian Fund for Applied Sciences (Fondo Italiano per le Scienze Applicate, FISA) and in part by Project RAILS "Robotic AI Solutions for Intelligent Railway Maintenance in Rolling Stock" under Grant FISA-2024-00232 – CUP J53C24005090001 funded by the Italian Ministry of University and Research (MUR). This article was recommended for publication by Associate Editor E. De Momi and Editor P. M. Wensing upon evaluation of the reviewers' comments. *(Corresponding author: Ali Khalilian-Motamed Bonab.)*

This work involved human subjects or animals in its research. Approval of all ethical and experimental procedures and protocols was granted by Scuola Superiore Sant'Anna Review Board under Application No. 41-2023, and performed in line with the 1964 Declaration of Helsinki.

The authors are with the Institute of Mechanical Intelligence and Department of Excellence in Robotics & AI, Scuola Superiore Sant'Anna, 56127, Pisa, Italy (e-mail: ali.khalilianmotamedbonab@santannapisa.it).

This article has supplementary downloadable material available at https://doi.org/10.1109/TRO.2026.3653884, provided by the authors.

Digital Object Identifier 10.1109/TRO.2026.3653884

© 2026 The Authors. This work is licensed under a Creative Commons Attribution-NonCommercial-NoDerivatives 4.0 License. For more information, see https://creativecommons.org/licenses/by-nc-nd/4.0/

comfortable human-suit interfaces; enabling robust control performance by addressing hardware-induced dynamic uncertainties and constraints; and constructing intuitive models to capture exosuit dynamics and its interaction with the user.

Cable-driven actuation systems are widely favored for their lightweight, low-profile design and precise controllability. However, they suffer from mechanical inefficiencies caused by friction losses in the tendon-sheath system, the compliance of the tendons themselves, and nonlinear behaviors like hysteresis, stick-slip, and backlash [47], [48], [49], [50], [51]. These issues are further compounded by the fact that tendon-driven exosuits inherently feature highly noncollocated actuation, which imposes fundamental limitations on their performance and coupled stability [52], [53]. These hardware-induced limitations directly degrade control performance, introducing dynamic uncertainties, phase lag, and bandwidth constraints that cannot be fully addressed by advanced control algorithms alone. For example, in tendon-driven exosuits employing cascaded admittance controllers, phase lag, and resonant modes between sensors and actuators can further destabilize the system [26], [54]. Enhancing the system's stiffness and addressing these internal resonances are essential to improve control precision and system efficiency.

In addition to the actuation system, the human–exosuit interface itself plays a critical role in system performance. Soft interfaces conform to the user's limb and improve comfort, but they also deform under load, absorbing assistive forces and introducing compliance that degrades control performance [55], [56]. On the other hand, rigid interfaces limit deformation and improve force transmission, but can cause discomfort and misalignment. Slippage at the interface further degrades performance by shifting the force application point, invalidating geometric parameters used by the controller, and reducing system stability [50], [57], [58]. Furthermore, concentrating the applied force at a single point worsens this slippage by creating high local pressure and reducing the effective friction between the interface and the limb. While solutions, such as active cuffs [59] and smart fabric designs [60] are promising, it is essential to develop a solution that minimizes deformation under load, comfortably conforms to the wearer's limb, and distributes forces over a larger area to reduce concentrated pressure. Such a design should also enhance friction at the interface and reduce slippage, all while maintaining user comfort. Due to these inherent hardware limitations, current systems often require subject-specific tuning of control parameters to achieve acceptable performance. However, this individualized calibration is impractical in real-world clinical or occupational scenarios, where plug-and-play usability and reliability across users are critical. Therefore, achieving robust and reliable assistance requires a mechatronics approach that improves the mechanical system to enable high-performance control. This would lead to a high-performing, efficient system that supports generic control strategies without relying on subject-specific adjustments.

To address these interconnected challenges, we developed a lightweight, portable, hybrid soft-rigid elbow exosuit that improves the performance and comfort of soft exosuits by incorporating mechanical stability and performance features inspired by rigid exoskeletons. Our design emphasizes minimizing hardware-induced inefficiencies to enable robust control and user comfort without relying on complex subject-specific adjustments. The main theoretical and hardware contributions of this work are as follows.

1) Development of a lumped-parameter model that captures the dynamics of the exosuit and its interaction with the human body, enabling design validation and performance optimization.
2) Design of a tendon-driven actuation unit paired with a compliant cuff interface that enhances force transmission while preserving comfort and adaptability.
3) Implementation of a dual-cabling architecture to reduce concentrated shear forces and minimize interface slippage.
4) Integration of a passive feeder mechanism that maintains proper cable tension throughout movement without increasing mechanical complexity.

The lumped-parameter model was developed to systematically capture the dynamic behavior of the exosuit and its interaction with the human body. This model provided intuitive insights into how design parameters affect system performance and stability. It also offered analytical validation that guided the mechanical design of the system and informed key tradeoffs to optimize performance. Our proposed system features a redesigned tendon-driven actuation unit paired with a compliant cuff interface that is specifically designed to balance comfort and mechanical performance. This cuff conforms to the wearer's limb for comfort and adaptability, while its geometry and stiffness around the force application points minimize deformation under load. This ensures that assistive forces are transmitted directly and efficiently to the human limb, reducing undesired cuff bending and compliance dynamics that would otherwise degrade control performance. To further support the compliant cuff interface, we implemented a dual-cabling architecture that distributes forces across two tendons, reducing concentrated pressure at anchor points and minimizing slippage. Elevated anchor points help preserve an optimal moment arm throughout the entire elbow range of motion (ROM), ensuring that assistive forces translate effectively into joint torque while minimizing shear loads that could compromise comfort or stability. Finally, to address cable slack, a common issue in tendon-driven systems, we developed a novel passive feeder mechanism that maintains consistent cable tension throughout all movement phases. Unlike semiactive solutions that increase complexity, our approach achieves these goals through a simple, reliable design that does not require continuous pretensioning forces, preserving user comfort.

In addition to the theoretical and hardware contributions, we developed a comprehensive human-subject evaluation protocol to assess the real-world performance of the exosuit. Our evaluation includes dynamic tasks that engage the elbow, shoulder, and wrist, offering deeper insights into how assistive forces impact muscle coordination across the entire arm. We also adapted endurance testing methodologies from lower limb exosuits to evaluate metabolic cost and muscle activation patterns during prolonged use, providing a rigorous assessment of the device's functional impact. Finally, to simulate realistic deployment scenarios, we implemented a generic interaction controller with

fixed parameters across all participants, deliberately avoiding subject-specific tuning. This approach reflects the practical constraints of clinical and occupational environments, where individualized calibration is often not feasible. While this generic strategy introduces greater intersubject variability, it demonstrates the system's readiness for real-world application and highlights the potential for future work on user-silent personalization techniques.

II. Methodology

A. Biomechanical Foundation

Understanding elbow anatomy and biomechanics is critical for designing assistive devices like exosuits. The elbow links the upper-arm and forearm, enabling hand positioning for tasks, such as grasping and lifting. Its stability and ROM facilitate essential movements like flexion, extension, and pronation–supination.

Although traditionally modeled as a simple hinge joint with a fixed axis of rotation, recent studies reveal that the elbow functions as a "loose hinge," with a variable axis of rotation following a double quasi-conical frustum [61]. This variability depends on factors, such as motion type, forearm position, and applied torque [62], [63].

The functional ROM for most daily tasks is 30–120 degrees [64], with flexion–extension velocities averaging 268–417°/s during typical and work-related tasks [65] while athletic activities can demand extension speeds of up to 2700°/s [66]. In addition to kinematic demands, the daily tasks require elbow moments averaging 1 N-m, peaking at 4.45 N-m [67].

B. Theoretical Foundation

To gain a deeper understanding of the internal dynamics of the exosuit and its interaction with the human body, it is highly beneficial to develop a model that captures both the behavior of the exosuit and its integration with the human system. While lower limb exosuits benefit from established patterns of joint kinematics and dynamics during activities like walking [55], [56], the lack of consistent patterns for upper limb movements makes modeling and evaluation more challenging.

Exosuits introduce nonlinearities, such as hysteresis, friction, and slack, complicating the development of comprehensive models. Analytical models for tendon-sheath systems [68], [69], [70] and their applications [71] often provide limited practical insights. A pragmatic alternative is the lumped-parameter mass–spring–damper model offering a simplified yet effective abstraction by capturing the dominant compliance and damping characteristics of the system. This modeling approach has been widely adopted for tendon-based actuation systems [72], [73]. Building on that body of work, we adopt the lumped parameter approach of Eppinger and Seering [52] to model the elbow exosuit, simplifying nonlinear effects into dampers and springs.

Our model represents the tendon-sheath actuation unit as a compliant unilateral transmission: cable forces are strictly tensile, and slack is prevented by the antagonistic routing on the motor pulley, during elbow flexion or extension one tendon always remains in tension while its counterpart is back-driven. Consequently, the transmission never enters compression, and the spring–damper pair and forces are defined only for the pulling direction. The load cell, positioned between the transmission endpoint and the exosuit interface, is modeled as a spring–damper system. Since the stiffness of the load cell is significantly higher than that of the transmission and the two springs are in series, the resulting equivalent elasticity is governed by the more compliant spring. Furthermore, as the damping of the sensor is comparatively negligible, the transmission and load cell can be simplified into a single equivalent spring–damper system. In addition, the mass of the transmission is considered negligible, further reducing complexity.

TABLE I
Parameters Used in the Theoretical Foundation for Modeling the Internal Dynamics of Coupled Exosuit

Parameter	Value	Unit	Description
m_m	0.268	kg	Motor linear equivalent mass
m_c	0.15	kg	Cuff mass
m_h	2	kg	Human mass
b_m	40	Ns/m	Motor linear equivalent damping
b_t	10	Ns/m	Transmission damping
b_c	5	Ns/m	Cuff damping
b_h	3	Ns/m	Human damping
k_t	5×10^5	N/m	Transmission stiffness
k_c	1×10^3	N/m	Cuff stiffness
k_h	300	N/m	Human stiffness

Human dynamics are modeled as a mass–spring–damper system, where the bony structure of the arm is represented as a rigid mass and the soft tissue as a compliant system. To focus on the internal dynamics of the exosuit and its interaction with the body, we grounded the soft tissue dynamics and replaced the bony structure with a fixed attachment point, simplifying the model from a tenth-order [see Fig. 1(b)] to a sixth-order characteristic polynomial, as illustrated in Fig. 1(a) and expressed in (1). The parameters listed in Table I were used to conduct numerical simulations of the system. These parameters were selected within physiologically and mechanically plausible ranges reported in literature. Specifically, the human impedance parameters were chosen within the ranges reported by the authors in [74] and [75], while the transmission stiffness was selected within the range characterized by Xiloyannis [42] for upper limb soft exosuits. The cuff stiffness was set to an intermediate value between the tendon stiffness and the human stiffness to represent the compliant behavior of the human–device interface

$$\frac{x_h}{F_m} = G(s),$$
$$G(s) = \frac{< \text{2nd-order numerator polynomial} >}{< \text{6th-order characteristic polynomial} >}. \quad (1)$$

The numerator and characteristic polynomials are detailed in (A1)–(A3) in the Appendix.

The system stability is constrained by the first resonance mode of the transmission dynamics, which limits the closed-loop bandwidth [52]. Increasing transmission stiffness ($k_t \uparrow$) shifts the first resonance mode to a higher frequency, enhancing both

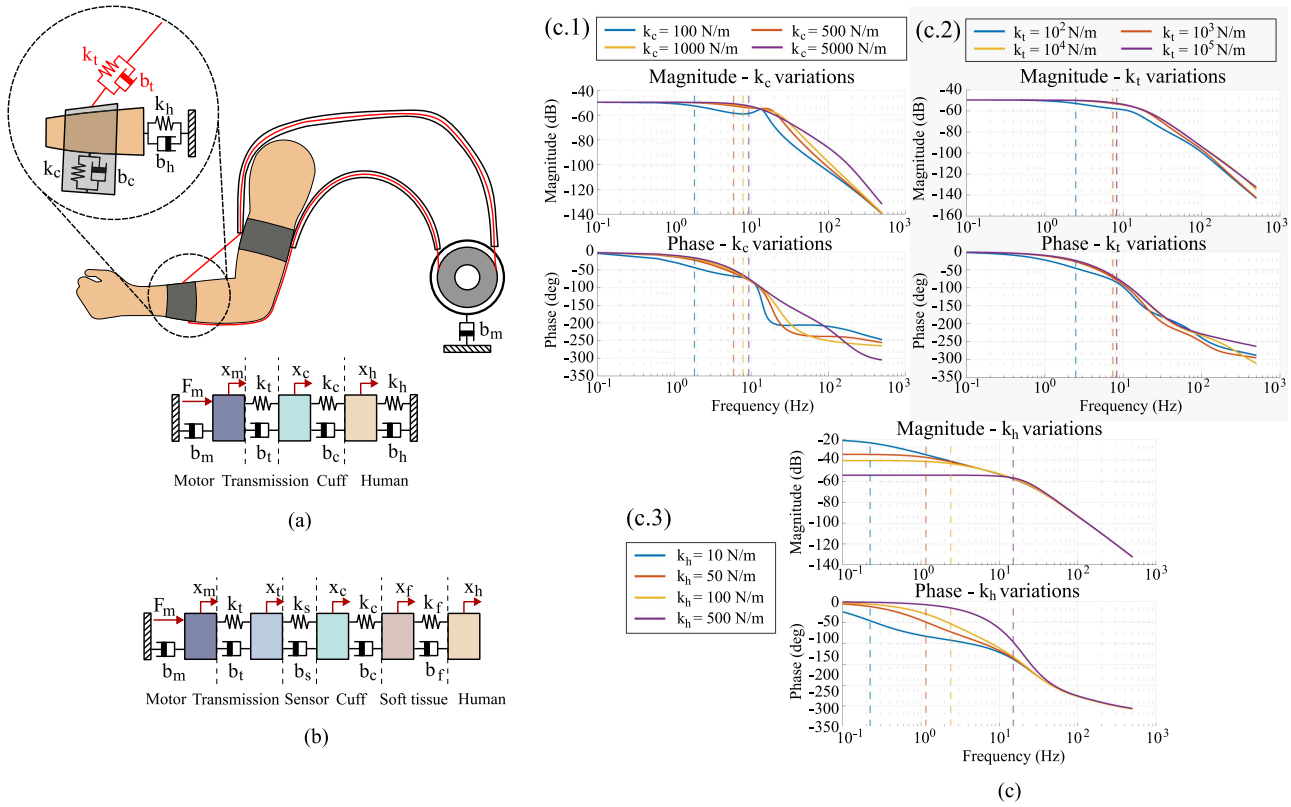

Fig. 1. (a) Simplified model of the soft exosuit and its interaction with the human body. (b) Detailed model of the exosuit and human interaction. Here, F_m represents the motor-applied force. Other parameters meaning is explained in Table I. (c) Bode diagrams of the coupled exosuit–human system under different stiffness values of the cuff (c.1), transmission (c.2), and human tissue (c.3). The bandwidth of each system is highlighted with a dashed line. (a) Simplified model of human–robot interaction. (b) Complex model of human–robot interaction. (c) Bode diagrams of HRI model.

the bandwidth and the stability margin. This relationship is qualitatively depicted in Fig. 1(c.2), showing bandwidth variations at low and high transmission stiffness.

In addition to stiffness, a high coefficient of transmission friction can improve stability margins but may cause input-dependent stability issues, such as limit cycles [76]. Similarly, increasing transmission damping ($b_t \uparrow$), which represents tendon-sheath friction in the lumped model, enhances stability but introduces time delays. Minimizing friction is therefore recommended and can be achieved by routing the transmission along the straightest path and reducing tendon-sheath contact.

Beyond the actuation unit, the interaction dynamics between the exosuit and the human interface can degrade system bandwidth [52]. In soft exosuits, cuff and interface dynamics notably impact performance, as shown empirically in [55] and [56]. Maximizing cuff stiffness ($k_c \uparrow$) while maintaining wearer comfort and minimizing damping ($b_c \downarrow$) enhances stability and bandwidth, as shown in Fig. 1(c.1). Attaching the exosuit to stiffer body parts, such as the bony sections of the forearm, further reduces dynamic interaction by increasing the stiffness of the body ($k_h \uparrow$), as illustrated in Fig. 1(c.3).

Although some of these design guidelines were initially proposed by Asbeck et al. [55], our model systematically verifies that implementing these recommendations significantly enhances the performance of the exosuit.

Specifically, in Fig. 1(c.1) we reported the effect of the cuff stiffness on the overall system (human–exosuit) bandwidth. This led us to design the hybrid soft-rigid exosuit to maximize bandwidth and meet human movement requirements based on theoretical simulation.

C. Exosuit and Actuation Unit Design Description

1) Actuation Unit Design: In line with the discussed design guidelines, the primary objective of the exosuit design was to enhance the actuation unit stiffness while minimizing parasitic effects. The actuation unit features a brushless electric motor (Cubemars AK80-9) with a 9:1 planetary reducer, delivering up to 9-N-m rated torque. An integrated servodrive and magnetic encoder enable precise low-level control and continuous position monitoring of the actuator.

The motor drives a 3-D-printed nylon pulley (20-mm radius, Onyx, Markforged material), as shown in Fig. 2(a) and (c), which manages an antagonistic cable configuration: two cables control elbow flexion, and two control elbow extension [Fig. 2(i)]. Power is transmitted via two pairs of Bowden cables made of 1-mm stainless steel with a PA-12 nylon coating (Stainless Steel Wire Rope AISI 316, 6 × 19 - WSC, PA 12 Coated, Carl Stahl), yielding high transmission stiffness and a minimum breaking force of 765 N.

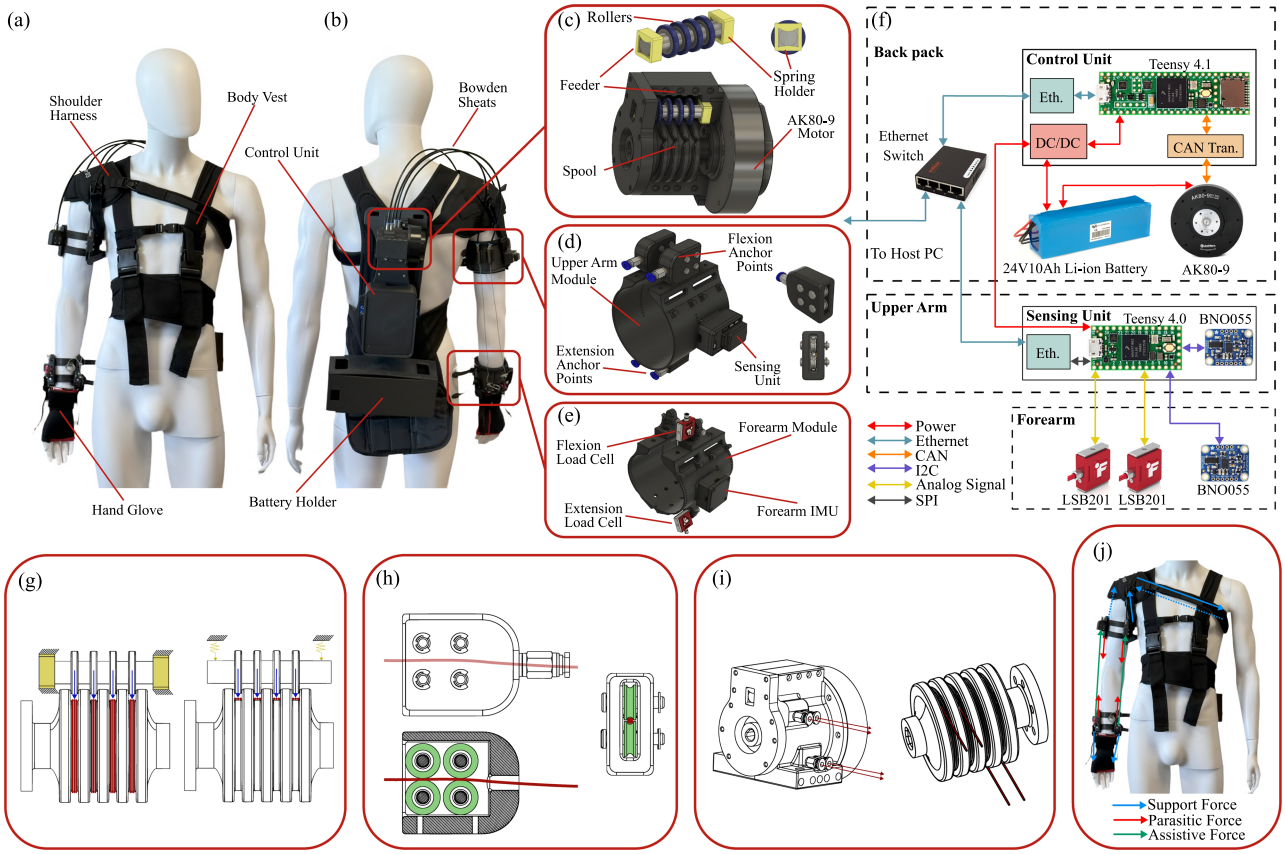

Fig. 2. Hybrid elbow exosuit mechanical and electrical description. (a) Front view of the exosuit showcasing its wearable structure. (b) Back view of the exosuit highlighting the backpack-mounted actuation unit and harness system. (c) Detailed mechanical design of the actuation unit and the passive cable feeder mechanism for tension maintenance. (d) Upper arm cuff with integrated guide mechanism ensuring smooth Bowden cable routing. (e) Forearm cuff design with ergonomic features and sensor integration. (f) The electrical architecture of the exosuit, illustrating the main control board located in the backpack, the data board on the upper arm cuff, and the sensor layout on the forearm cuff. (g) Schematic of the passive feeder mechanism illustrating spring forces acting on the spool to ensure consistent tendon tension. (h) Cross-sectional and front views of the guide mechanism showing how the tendon passes through ball bearings to minimize friction and misalignment. (i) Cable routing diagram displaying the antagonistic configuration of flexion and extension cables and their exit paths from the actuation unit. (j) Illustration of assistive and parasitic force vectors at the cuff interface, along with the corresponding support forces provided by the orthoses to counteract shear forces and minimize slippage.

To address backlash and cable slack, a novel passive tensioning mechanism was integrated directly into the pulley system. This tensioning device employs a compliant spring, a shaft, four rollers, and ball bearings, ensuring continuous pretensioning of the cables without relying on clutches or transmitting excessive forces to the user [Fig. 2(c) and (g)]. The spring is compressed against the feeder shaft, maintaining a consistent downward force. Rollers, precisely fitted to the pulley grooves, allow cables to wrap around the pulley three times, optimizing grip and tension. By independently operating feeders for flexion and extension cables, the mechanism compensates for discrepancies between cable pairs, ensuring smooth operation and preventing slack throughout the system.

In addition, the low gear reduction ratio of the motor and the minimal friction of the system provide passive back-drivability, ensuring mechanical transparency. This allows the exosuit to adapt naturally to the wearer's motion during nonactuated phases, enhancing user comfort and minimizing resistance.

2) Exosuit Unit Design: To ensure efficient power transfer from the actuation unit to the human body, the exosuit was designed with a focus on user comfort, adaptability, and minimizing slippage. The design consists of a back interface, shoulder harness, compliant upper arm, and forearm cuffs, and a custom hand brace, as shown in Fig. 2(a), (d), and (e).

The cuffs, serving as the primary human–robot interface, are designed to fit the cross-sectional geometry of the upper arm and forearm. They are 3-D-printed from a lightweight yet stiff nylon composite material (Onyx, Markforged) and reinforced at the power exchange points to enhance stiffness and prevent deformation under load. The cuffs include two anchor points for flexion and two for extension, which ensure an even distribution of assistive forces, minimizing concentrated pressure and shear on the wearer's skin.

To further enhance comfort and reduce slippage, the inner surfaces of the cuffs are lined with a 4-mm-thick layer of polyamide padding (ComforTex Grippy, Ottobock), selected for its antislip properties and air permeability. The cuffs are secured using nylon straps modeled after watch straps, allowing precise and secure fastening.

The dual-cable system employed in the cuff design reduces peak forces experienced by the subject. This reduction in peak force, coupled with the even distribution of forces across a larger

area of the upper arm and forearm, results in lower pressure on the wearer. The slippage between the cuffs and the skin is further reduced by the even distribution of shear forces and the antislip properties of the padding material. This effect follows a simple mechanical principle: applying a force at a single point concentrates shear stress, increasing the likelihood of local slippage. In contrast, distributing the same total force across multiple points lowers the stress at each location and increases the effective contact area, which enhances the frictional interaction between the cuff and skin. As a result, the distributed configuration reduces the risk of slippage.

The forearm cuff features an IMU for elbow angle estimation, four cable anchor points, and two load cells (LSB201, Futek) to monitor flexion and extension tendon tension [Fig. 2(e)]. To minimize slippage, a modified commercial hand brace (Hand Brace, AS-N-02, Reh4Mat) was added, and secured to the cuff via inextensible webbing bands with side-release buckles. Combined with the conical shape of the forearm and straps, this setup effectively mitigates shear forces and enhances stability [Fig. 2(j)].

The upper arm cuff integrates a custom electrical board with an IMU and four proximal cable anchor points. Bowden cables pass through these points, sheathed in low-friction housings (Jagwire, LEX-SL, ∅4 mm) to reduce friction during elbow flexion. This cuff is secured to a shoulder harness (Master-03, Reh4Mat) to transfer forces to the torso and prevent slippage [Fig. 2(j)].

Given the angular changes in the Bowden cables during elbow flexion, the cables tend to contact the structure at the proximal anchor point and with the inner layer of the sheath. To minimize friction, a novel guide mechanism was designed, as illustrated in Fig. 2(d) and (h). This mechanism includes four U-groove ball bearings, fitted into a housing with enough spacing to allow the Bowden cable to pass through with minimal tolerance. This design ensures that as the cable angle changes, the cable interacts with the ball bearings, reducing friction and preventing misalignment of the insertion angle.

Lastly, the back interface houses the actuation unit, electronics, and battery, ergonomically contoured for comfort and efficient torque transmission. Bowden cable sheaths are routed in a large, gentle curve to accommodate typical arm movements without a large deformation or resistance. The total weight of the exosuit is 4085 grams, with individual components contributing as follows: The orthoses weigh 195 grams, the actuation unit 880 grams, and the backpack with electronics 1250 grams. The upper arm cuff weighs 200 grams, while the forearm cuff is 160 grams. In addition, the battery accounts for 1400 grams of the total weight.

3) Electronics: The main electronics, mounted on the back interface, include a custom-made board with a Teensy 4.1 microcontroller, a 4-port Gigabit Ethernet switch (Roline), and the motor's integrated servo driver (CubeMars Driver Board-V2.2). A second custom board, the "Data Board," featuring a Teensy 4.0 microcontroller, is mounted on the upper arm cuff to collect data from load cells and IMUs (BNO 055) embedded in the board and on the forearm cuff. The system is powered by a 24 V, 10 Ah Li-Ion battery and interfaced with a laptop via Ethernet. The load cells were factory-calibrated by the manufacturer, and their output was verified before experiments to ensure consistent measurements.

The servo driver acts as a low-level controller, acquiring motor data (position, velocity, current) and communicating via controller area network (CAN) protocol with the main board. The main board executes the high-level control algorithm, sends commands to the motor driver, and processes incoming data. The data board collects sensor data (IMUs and load cells) and transmits it to the main board via Ethernet. Although a laptop was used during experiments for initiating the system, monitoring, and data logging, the controller itself is fully embedded in the exosuit and capable of running autonomously without external devices.

At the beginning of each use, the embedded IMUs were calibrated while the participant wore the exosuit. This process involved a brief sequence of arm movements to allow the system to initialize and correct for orientation offsets. The calibration was automatically validated by the controller before enabling assistance.

Both boards execute the high-level controller and communication at 500 Hz, and the measured control-loop latency is approximately 2 ms. Embedded code is written in C++, with MATLAB/Simulink used to interface with the main board.

4) Control Architecture: The controller, based on the design by Xiloyannis et al. [26], was adapted to assist by partially compensating for gravitational arm loads while minimizing interference with natural arm kinematics. The architecture employs a collocated admittance controller [77], with an outer loop for gravitational assistance and an inner velocity control loop (Fig. 3).

The torque due to gravity (τ_{gravity}) is modeled under the premise that the arm remains fully adducted, with minimal shoulder movement, as shown in the following equation:

$$\tau_{\text{gravity}} = mgl_f \sin(\theta) \tag{2}$$

where m, g, l_f, and θ are the combined mass of the forearm and load, gravitational acceleration, forearm center of mass distance, and elbow angle.

The assistive torque is computed using load cell data and moment arm calculations based on [78], doubling the measured force to account for the dual-cable design (4) and (5). In this context, J_{f}, J_{e}, and τ_{assist} represent the flexion Jacobian, extension Jacobian, and the assistive torque calculated using the load cell force (f_{loadcell}) and corresponding Jacobians, respectively. The specific parameters for these Jacobians are shown in Fig. 3.

$$J_{\text{f}} = \frac{-a_1a_2s_\theta - b_1b_2s_\theta - a_1b_2c_\theta + a_2b_1c_\theta}{\sqrt{(a_1 - a_2c_\theta + b_2s_\theta)^2 - (b_1 - a_2s_\theta - b_2c_\theta)^2}} \tag{3}$$

$$J_{\text{e}} = R_{\text{elbow}} \tag{4}$$

$$\tau_{\text{assist}} = J_{\text{exosuit}}^T \, f_{\text{loadcell}}. \tag{5}$$

Although subject-specific measurements were collected, the controller was implemented using fixed geometric parameters across participants ($a_1 = 150$ mm, $a_2 = 120$ mm, $b_1 = 70$ mm,

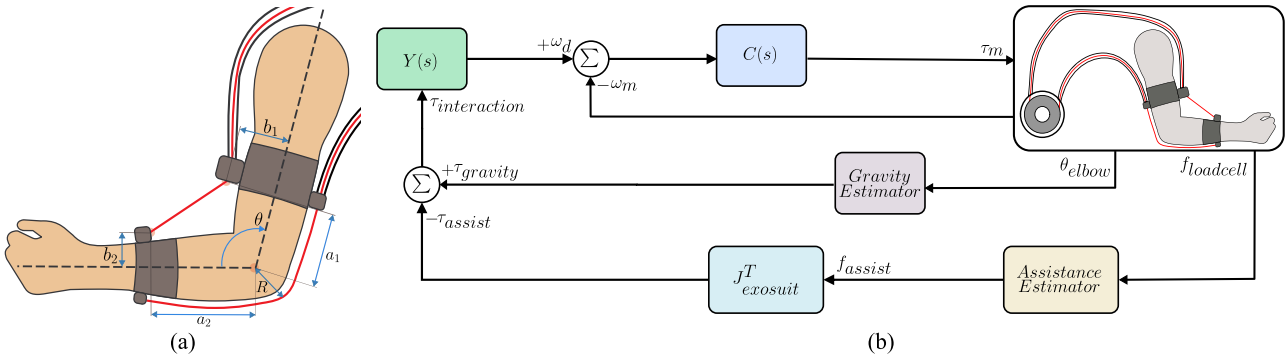

Fig. 3. (a) Geometric model of the exosuit with defined parameters used to compute the Jacobian. Note that the routing shown corresponds to the condition where the flexion cable is engaged and the extension cable is slack, which explains the routing of the extension cable. (b) Block diagram of the collocated admittance controller for transparency and gravity compensation.

TABLE II
CONTROL PARAMETERS FOR THE ADMITTANCE AND VELOCITY PID CONTROLLERS

Parameter	Value (Unit)	Parameter	Value (Unit)
K_{p_a}	10 (rad·s^{-1}/Nm)	K_{p_v}	0.375 (Nm/rad·s^{-1})
K_{d_a}	0.002 (rad·s^{-2}/Nm)	K_{d_v}	0 (Nm·s/rad)
K_{i_a}	0.002 (rad/Nm)	K_{i_v}	0.05 (Nm/rad)

$b_2 = 75$ mm, $R = 80$ mm), as the cuff design and their attachment to the orthoses minimize intersubject variability.

Interaction torque ($\tau_{\text{interaction}}$), derived from the difference between τ_{gravity} and τ_{assist}, is used to compute the reference velocity for the inner control loop (6) via an admittance controller (7)

$$\omega_d(s) = Y(s)\tau_{\text{interaction}} \tag{6}$$

$$Y(s) = Kp_a + Kd_a s + Ki_a/s. \tag{7}$$

Here, Kp_a, Kd_a, and Ki_a define the proportional, derivative, and integral terms that regulate the dynamics between the interaction force and the exosuit's kinematics. The computed reference velocity is then fed to the velocity control loop, which in turn determines the motor's reference torque, governed by the velocity controller shown as follows:

$$C(s) = Kp_v + Kd_v s + Ki_v/s. \tag{8}$$

The PID parameters for admittance and velocity controllers were tuned based on prior recommendations [54], [79] and fine-tuned for experiments (Table II).

The exosuit's mechanical design ensured consistent performance across subjects by attenuating wearer-specific dynamic variations, eliminating the need for subject-specific controller tuning. While individual tuning could enhance performance, we used uniform parameters to evaluate the exosuit's baseline functionality without fine-tuning. Subject-specific tuning, though beneficial, is technically complex, requiring significant training and time, which can limit practicality in clinical settings. Therefore, designing a robust exosuit capable of delivering effective assistance without tuning is more suitable for broader usability and clinical adoption.

III. EXPERIMENTAL PROCEDURE

The exosuit was evaluated in two categories: 1) performance characterization and 2) its effects on human kinematics and biomechanics, conducted across two separate seating. The protocol is depicted in Fig. 4. The biomechanical experiments included two sessions: 1) the dynamic session [with subtasks of pick and place (P & P) as shown in Fig. 4(d), and pick, lift, and place (P, L, & P) as shown in Fig. 4(e)] and 2) the Endurance Session [Fig. 4(f)]. Notably, the interaction controller, gravity assistance, and the Jacobian parameters were kept fixed across participants to assess the exosuit's performance and biomechanical impact under a standardized configuration, without subject-specific tuning.

A. Participants

The biomechanical experiments were conducted with ten healthy participants (nine male and one female, age: 29.7 ± 2.75 years, height: 178 ± 6.32 cm, weight: 77.3 ± 10.01 kg, mean ± std) while characterization experiments were conducted with a subset of 5 participants selected randomly. All participants were right-handed, self-reported no neurological, chronic, or physical impairments, and had no metabolic or cardiopulmonary instability.

Participants were instructed to avoid alcohol, energy drinks, and heavy exercise 24 h before the biomechanical sessions, refrain from caffeine, and avoid heavy meals 6 and 2 h prior to the experiments. They were briefed on the procedures before the sessions and provided informed consent. The protocol was reviewed and approved by the Scuola Superiore Sant'Anna Review Board, approval number 41-2023.

B. Exosuit Characterization

In order to characterize the performance of the exosuit three sets of experiments were performed that characterize the bandwidth of the exosuit, ROM, and comfort of wearers. Each experiment is discussed in the following sections.

1) Exosuit Comfort Experiment: Comfort was evaluated by measuring the pressure distribution at the anchor points (cuffs) under varying gravity assistance levels. Pressure sensors (A502,

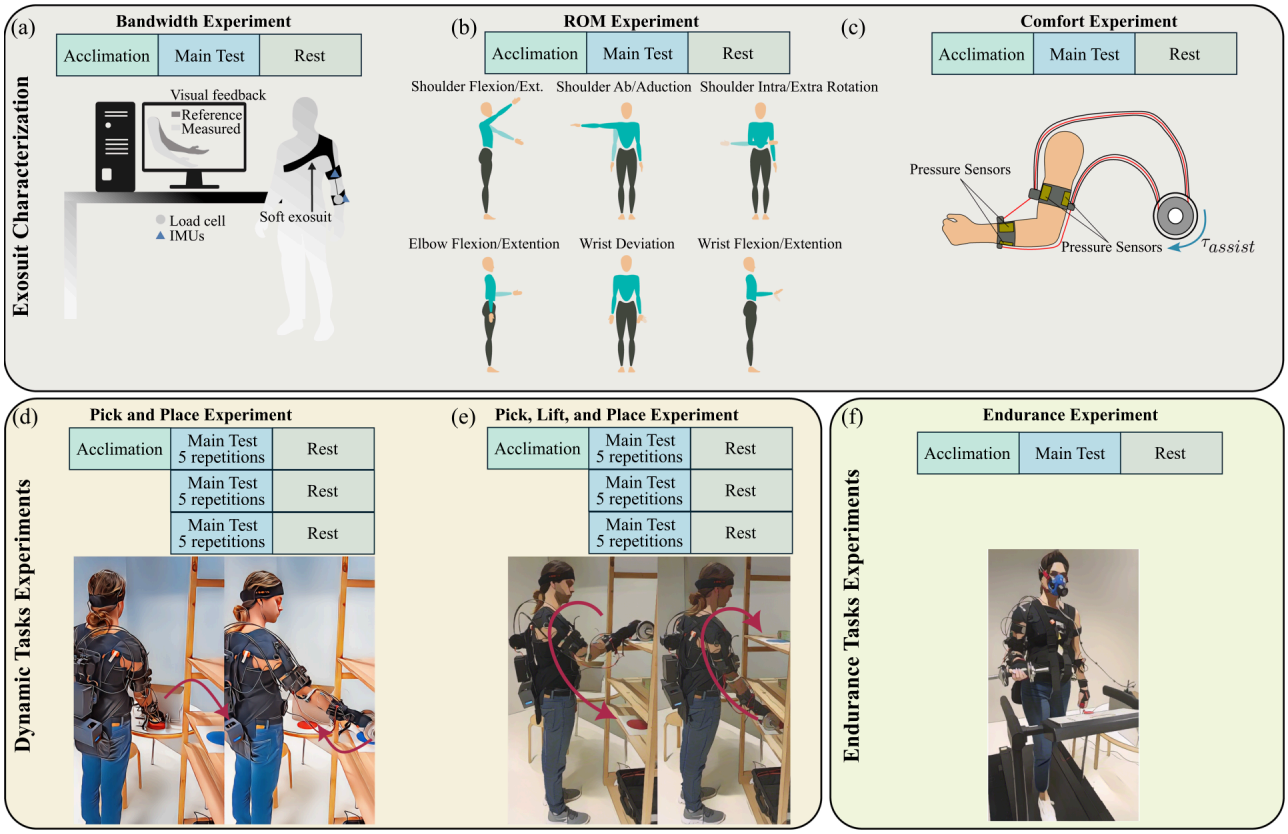

Fig. 4. Overview of the experimental procedure. (a) Protocol and schematic for the HIL closed-loop control bandwidth experiment. (b) Protocol and schematic for the ROM and transparency experiment. (c) Protocol and schematic for the Exosuit Comfort experiment. (d), (e) Protocols and schematics for the P & P and pick, lift, and place (P, L, & P) tasks within the dynamic session. (f) Protocol and schematic for the Endurance session experiment.

Tekscan) were placed between the skin and cuffs, and pressure was recorded while participants held their arm at a 90° angle, maximizing gravitational force on the forearm's posterior side.

Assistance levels ranged from 0–3 kg in 0.5-kg increments. After a brief acclimation phase, participants repeated the experiment with a reconfigured sensor placement, as shown in Fig. 4(c).

2) Human-in-The-Loop Closed-Loop Control Bandwidth Experiment: System bandwidth was assessed by tracking a sinusoidal reference trajectory (9) with 0.5-kg gravity assistance. The trajectory amplitude covered typical elbow ranges for daily tasks ($A_0 = 50°$ and $A_1 = 40°$), with frequencies ranging from 0.05–1.5 Hz, corresponding to velocities from 18 to 540 deg/s.

$$\theta_d(t) = A_0 + A_1 \sin(2\pi f t). \tag{9}$$

After an acclimation phase, during which participants familiarized themselves with the task, the main experiment began. Each participant experienced 30 s at each frequency, with the last five full cycles used to capture the steady-state response.

The bandwidth was calculated using the root mean square (RMS) ratio of measured and desired elbow angles (10). The magnitudes for each frequency across all participants were averaged, and the "System Identification Toolbox" of MATLAB (MathWorks, 2023b) was used to fit a second-order system, to the experimental data

$$C_f(\theta) = \frac{\text{RMS}(\theta_m)}{\text{RMS}(\theta_d)}. \tag{10}$$

The quality of the fit was assessed using the coefficient of determination R^2, and the root mean squared error (RMSE) between the model and the experimental data.

3) Range of Motion Experiment: This experiment tested the hypothesis that the active mode of the exosuit does not impede the wearer's movements. Participants performed full shoulder, elbow, and wrist motions under two conditions: a) no exosuit; and b) exosuit power-on. Movements included flexion/extension, abduction/adduction, and radial/ulnar deviation, as illustrated in Fig. 4(b). The ROM for each degree of freedom was recorded and compared between the two conditions to assess the effect of the exosuit on wearers' ROM. While these measurements do not capture the full effort or muscle activation required to achieve these movements, they help determine whether the exosuit mechanically restricted motion in the powered-ON condition.

C. Dynamic Session

The dynamic session assessed the exosuit's performance in providing gravitational assistance while shadowing the wearer's movements. Two dynamic tasks were developed to activate

different sets of muscles, allowing for an exploration of the exosuit's performance across varying dynamic movements and muscle coordination patterns. These tasks are referred to as P&P and P, L, &P. Such tasks offer a more holistic evaluation of the exosuit's effect on arm coordination and muscle activity, rather than focusing solely on the joint of interest. This design enabled us to investigate whether participants altered their arm coordination across different conditions to accomplish the required tasks.

In the P&P task, participants moved a 3.5-kg weight between two locations with a 20-cm height and 90-cm lateral difference, using only arm movements. The P, L, &P task involved lifting the weight 60-cm vertically before placement. Both tasks activated multiple degrees of freedom, with the P, L, & P task emphasizing flexion/extension at the shoulder, elbow, and wrist.

Experiments were conducted under three conditions: 1) no exosuit; 2) exosuit powered OFF; and 3) exosuit powered ON. In the powered-OFFcondition, the actuation system was disabled, and the device behaved passively without generating any assistive torque. After acclimation, participants completed three trials of five repetitions per task per condition, with randomized conditions and rest breaks to minimize fatigue and learning effects. Tasks were performed at a self-paced speed.

TABLE III
SYSTEM USABILITY SCALE (SUS) QUESTIONS WITH CORRESPONDING ABBREVIATIONS

Abbreviation	SUS Questions
Overall Satisfaction	I think that I would like to use this system frequently.
Complexity	I found the system unnecessarily complex.
Ease of Use	I thought the system was easy to use.
Need for Support	I think that I would need the support of a technical person to use this system.
Functionality Integration	I found the various functions in this system were well-integrated.
Inconsistency	I thought there was too much inconsistency in this system.
Learnability	I would imagine that most people would learn to use this system very quickly.
Cumbersomeness	I found the system very cumbersome to use.
Confidence	I felt very confident using the system.
Learning Requirement	I needed to learn a lot of things before I could get going with this system.

D. Endurance Session

The endurance session examined muscle coordination, metabolic rate, and fatigue while participants carried a 3.5-kg weight with their elbow at a 90° angle during treadmill walking. After acclimation, participants selected a comfortable walking speed, maintained throughout the session.

Participants walked under three randomized conditions for at least 4 min each: 1) baseline (no weight or exosuit); 2) weight only; and 3) weight with exosuit assistance. Rest intervals of at least 5 min mitigated fatigue. Baseline measurements assessed walking metabolic cost, while the other conditions evaluated muscle activity, metabolic cost, and fatigue during load carriage with and without assistance.

E. Performance Metrics

1) Muscle Activity: The electromyography (EMG) was recorded from key muscles involved in the shoulder (Deltoid: Anterior, Posterior, Middle; Infraspinatus), elbow (Triceps Long Head, Biceps Short Head, Brachioradialis), and wrist motion (Extensor Carpi Ulnaris, Flexor Carpi Radialis) using wireless surface EMG sensors (Delsys, Trigno) by following electrode placement guidelines in [80]. Signals were acquired at 2148.1 Hz, processed (band-pass filtered at 30–450 Hz, rectified, low-pass filtered at 6 Hz using a zero-phase second-order Butterworth filter), and normalized to maximum voluntary contractions (MVC) measured at session start and end of experimental seating. Finally, abnormal peaks and artifacts were manually removed from signals to avoid alterations in metrics computation and statistics.

2) Metabolic Cost: The metabolic cost of participants was measured using indirect calorimetry (K5, Cosmed). The rates of carbon dioxide production ($\dot{V}CO_2$) and oxygen consumption ($\dot{V}O_2$) were averaged over a one-minute span from minute 3 to minute 5 during the 4-min (minimum required) walking period for each condition. These values were then used to calculate metabolic rate using the Brockway equation [81], as expressed in the following equation:

$$\overline{P} = 16.58 \times \overline{\dot{V}}_{O_2} + 4.51 \times \overline{\dot{V}}_{CO_2}. \tag{11}$$

3) Joint Kinematics: Arm kinematics were recorded using inertial measurement units (IMUs) provided by the Xsens MVN Link system (Xsens Technologies B.V.). Each participant was equipped with 11 IMUs placed on the hands, forearms, upper arms, scapula, sternum, head, and pelvis, according to the guidelines outlined in the Xsens MVN manual. The IMU signals were sampled at 240 Hz, and data were collected using the MVN Analyze 2022.0.2 software (Xsens Technologies B.V.).

4) Qualitative Assessment: In addition to quantitative measurements, subjective assessments were collected from participants to evaluate their perception of the exosuit and the usability of the system. To assess the perceived workload of each condition in both the dynamic and endurance sessions, participants completed the *NASA Task Load Index* questionnaire, which evaluates mental demand (MD), physical demand (PD), temporal demand (TD), performance (PR), effort (EF), and frustration (FR). Participants also completed the *System Usability Survey* (SUS) [82] (Table III), which consists of ten statements regarding device usability and an SUS score from 0 to 100 was obtained for each participant following the method presented by Brooke [82]. Both questionnaires were rated using a five-point Likert scale (ranging from "strongly disagree" to "strongly agree").

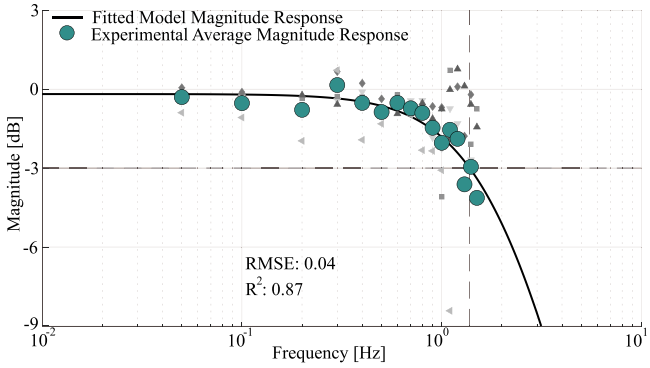

Fig. 5. Bode plot of the estimated transfer function between the measured and desired elbow position. The human–exosuit system demonstrates a bandwidth of 1.37 Hz, highlighted by the dashed line. Grey markers represent individual subject data, while green circles indicate the averaged experimental magnitude data across all participants.

F. Data Processing and Statistics

Data from all sources were synchronized using a single host PC. Each subject performed two dynamic tests (three trials with five task repetitions per trial) and one endurance test (single trial per condition). For dynamic tests, interrepetition rest phases were removed manually, and the RMS metric was computed for EMG (all muscles) and IMU (position, velocity, and acceleration) data, averaged across repetitions. Spectral arc length (SPARC) and ROM metrics were calculated from IMU signals [83]. Statistical comparisons of metrics across no-exo, exo-off, and exo-on conditions used one-way analysis of variance (ANOVA) for normal data distributions, and Kruskal–Wallis tests for nonnormal data distributions, with a significance threshold of $p = 0.05$. Paired ANOVA or Kruskal–Wallis tests were used in case of significant differences found in the group.

For endurance tests, metrics included time evolution (slopes from 10-s RMS windows) and a 20-s RMS window after 4 min. For this test, EMG signals and calorimetry data were analyzed: EMG metrics were calculated for all muscles, while calorimetry focused on VO2 and VCO2 measurements. Statistical comparisons between no-exo, no-exo unloaded, and exo-loaded conditions were performed using one-way ANOVA for normal data and the Mann–Whitney test for nonnormal data, with a significance threshold of $p = 0.05$. Paired ANOVA or Kruskal–Wallis tests were used in case of significant differences found in the group. The normality of data distributions was assessed with the Shapiro–Wilk test. Effect sizes (Cohen's d for paired comparisons) were additionally reported for ROM and EMG metrics whenever statistically significant differences were detected.

IV. Results

A. Exosuit Characterization

Fig. 5 shows the magnitude Bode plot comparing experimental data (green circles) and the fitted second-order model (black line) across frequencies from 0.05 to 1.5 Hz. The model aligns closely with experimental data ($R^2 = 0.87$, RMSE $= 0.04$).

TABLE IV
Range of Motion for Different Joints With and Without the Exosuit. Values are Reported as Mean ± Standard Deviation

Joint	Without Exosuit [deg]	With Exosuit [deg]
Shoulder Flexion	138.75 ± 25.03	113.51 ± 33.73
Shoulder Abduction	122.01 ± 16.58	104.56 ± 21.17
Elbow Flexion	149.20 ± 9.99	135.15 ± 12.17
Wrist Flexion/Extension	117.46 ± 17.51	112.79 ± 30.33
Radio-ulnar Deviation	44.25 ± 21.94	40.86 ± 18.24

The system bandwidth, defined at −3-dB gain, is 1.37 Hz, corresponding to a peak velocity of 493 °/s. This indicates that the system can effectively track movements within the range of typical daily activities and partially cover work-related tasks. The cutoff frequency aligns with the expected performance goals of the exosuit, supporting its design for enhanced system bandwidth. It should be noted that Fig. 1 shows the simulated lumped-parameter model, whereas Fig. 5 reports the experimentally measured system; therefore, these two results are not directly comparable.

The pressure distribution of the exosuit on the skin is shown in Fig. 6, detailing the pressures exerted by the forearm and upper arm cuffs under varying assistance levels and in the no-assistance condition. In the no-assistance condition, baseline pressures averaged 5.13 ± 1.30 kPa and 5.16 ± 1.11 kPa at the forearm and upper arm anchor points, respectively, resulting from the attachment of the exosuit.

Maximum pressures occurred during 3-kg gravity assistance with the hand at a 90 ° angle, where the gravitational load on the arm was highest on the posterior forearm. Under these conditions, the forearm and upper arm cuffs exerted pressures of 19.21 ± 3.46 kPa and 15.34 ± 1.12 kPa, respectively, while anchor points experienced pressures of 12.93 ± 4.44 kPa (forearm) and 6.34 ± 1.12 kPa (upper-arm).

In the ROM analysis, there was a slight reduction in ROM across all joints when using the exosuit, with considerable variability observed between subjects. Shoulder flexion decreased from 138.75 ± 25.03° without the exosuit to 113.51 ± 33.73° with the exosuit, and shoulder abduction reduced from 122.01 ± 16.58 to 104.56 ± 21.17°. Elbow flexion decreased from 149.20 ± 9.99° to 135.15 ± 12.17°, while wrist flexion/extension and radio-ulnar deviation decreased slightly from 117.46 ± 17.51° to 112.79 ± 30.33° and from 44.25 ± 21.94° to 40.86 ± 18.24°, respectively. This data are summarized in Table IV.

B. Performance of Exosuit

Fig. 7 presents the results for the dynamic session experiments during the P & P and P, L, & P tasks. In the P & P task, biceps activity was significantly reduced with powered assistance (3.36 ± 1.85 % MVC) compared to no-exosuit (4.98 ±2.45 % MVC, $P < 0.01$, $d = 0.80$), representing a 28.40% average reduction and powered-OFFconditions (4.56 ± 2.65 % MVC, $P < 0.05$, $d = 0.89$) by 23.58% average reduction. Similarly, during the P, L, & P task, biceps activity decreased significantly with assistance (4.20 ± 3.05 % MVC) compared to

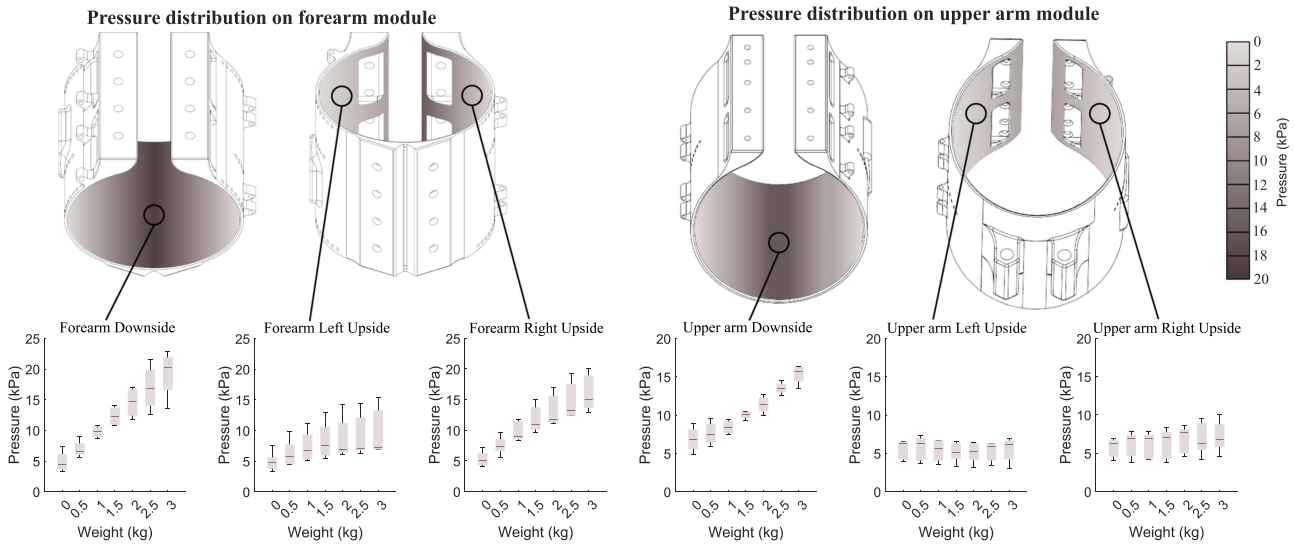

Fig. 6. Pressure distribution characterization at the human-suit interface: Measured pressures at the upper-arm and forearm cuffs under varying assistance levels under a 90 ° elbow bend. "Upside" and "Downside" in the figure refer to the upper and lower regions of each cuff, respectively.

no-exosuit (5.60 ± 3.85 % MVC, $P < 0.01$, $d = 0.64$) by 33.72% and powered-OFFconditions (5.56 ± 3.65 % MVC, $P < 0.05$, $d = 1.01$) by 32.06% . Flexor carpi ulnaris activity was significantly lower with assistance in the P, L, & P task ($P < 0.05, d = 1.17$), showing an average reduction of 30.55%, while triceps activity remained unaffected, indicating robust interaction control. Middle deltoid activity increased significantly in the powered-OFFcondition compared to no-exosuit during the P & P task ($P < 0.01, d = -0.94$) by 14.76% average increase.

In the P, L, & P task, the ROM in the no-exosuit condition was 48.38 ±11.97° for shoulder flexion, 37.82±9.37° for shoulder rotation, 103.85±13.85° for elbow flexion, and 51.82±13.30° for wrist flexion. Compared to this baseline, ROM was significantly reduced with powered assistance for shoulder flexion (35.52 ± 9.87°, $P < 0.001$, $d = 0.89$), shoulder rotation (25.21 ± 5.19°, $P < 0.001$, $d = 1.28$), elbow flexion (88.89 ± 9.94°, $P < 0.001$, $d = 1.35$), and wrist flexion (43.27 ± 14.36°, $P < 0.05$, $d = 0.51$). In the powered-OFFcondition, significant differences were observed for shoulder flexion (38.47 ± 7.81°, $P < 0.001$, $d = 0.79$), shoulder rotation (23.94 ± 7.19°, $P < 0.001$, $d = 1.23$), and elbow flexion (94.06 ± 6.69°, $P < 0.001$, $d = 0.73$). For the P & P task, shoulder flexion ROM in the no-exosuit condition was 40.45 ± 11.04° and reduced with powered assistance (28.79 ± 6.75°, $P < 0.001$, $d = 1.28$), while shoulder rotation was significantly different in the powered-OFFcondition (25.47 ± 10.04°, $P < 0.001, d = 1.77$) compared to no-exosuit condition (43.82 ± 10.42°).

Smoothness, measured by SPARC, was unaffected during the P & P task but decreased significantly for shoulder movements in the P, L, & P task in the powered-ON (−4.30 ± 0.62 SPARC, $P < 0.05$) and powered-OFFconditions (−4.38 ± 0.50 SPARC, $P < 0.05$). Hand smoothness was significantly lower in the powered-OFFcondition compared to no-exosuit (−3.30 ± 0.28 SPARC, $P < 0.01$), whereas forearm smoothness improved with powered assistance (−3.86 ± 0.35 SPARC, $P < 0.05$) compared to both powered-OFF (−3.61 ± 0.29 SPARC) and no-exosuit conditions (−3.68 ± 0.26 SPARC).

RMS segment accelerations were significantly reduced across all conditions with the exosuit ($P < 0.001$), with the lowest values observed in the powered-ON condition ($P < 0.001$). Forearm acceleration was significantly lower with powered assistance compared to powered-OFFconditions in both tasks.

During the endurance session, participants walked on a treadmill at an average speed of 0.67 ± 0.16 m/s, which was significantly lower than typical walking speeds reported in literature [84]. Carrying a load without exosuit assistance led to a significant increase in average muscle activity and its slope across all targeted muscles compared to baseline (walking without a load, $P < 0.001$).

With exosuit assistance, the average muscle activity during load carriage remained largely comparable to the no-assistance condition, except for the infraspinatus muscle, which exhibited an average reduction of 44.55% (1.86 ± 0.90% MVC vs. 3.35 ± 1.60% MVC, $P < 0.05, d = 1.04$). In addition, the slope of deltoid middle muscle activity was significantly lower with exosuit assistance (0.47 ± 0.34% MVC) compared to the unloaded no-assistance condition (1.30 ± 0.49% MVC, $P < 0.01$, $d = 0.90$). The exosuit also reduced activity in the triceps, extensor carpi radialis, and flexor carpi radialis compared to the loaded no-assistance condition. While these reductions were not statistically significant, the exosuit effectively prevented significant increases in activity relative to the unloaded no-assistance condition.

The metabolic consumption and its slope, as shown in Fig. 8, were consistent across conditions, with no significant differences observed. Similarly, the central spectrum frequency, an indicator of muscle fatigue, showed no significant impact from the exosuit in most muscles. However, for the infraspinatus muscle, the central frequency indicated reduced fatigue with

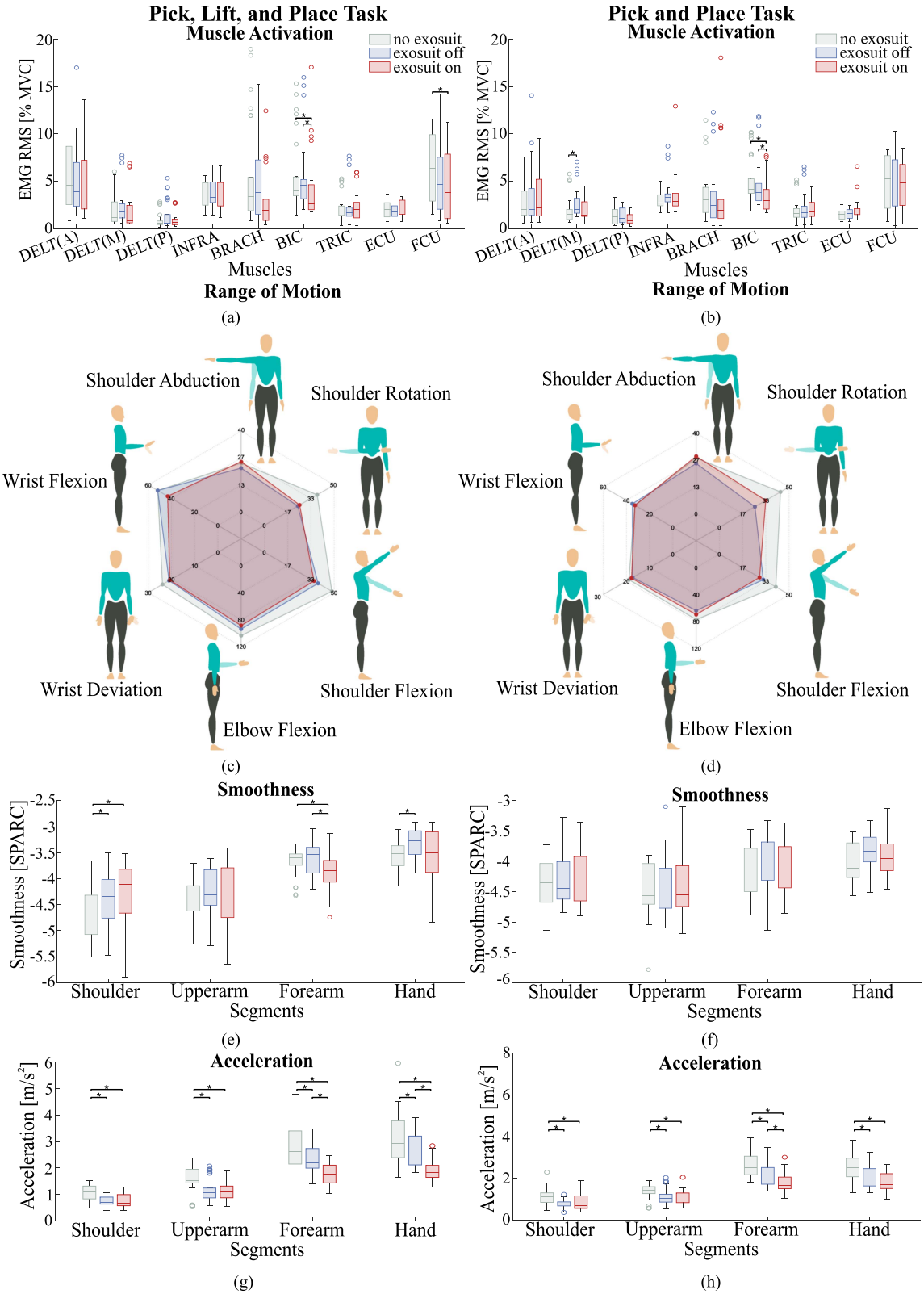

Fig. 7. Comparison of muscle activation (a), (b), ROM (c), (d), smoothness (e), (f), and acceleration (g), (h) across participants in three experimental conditions during P, L, & P and P & P tasks within Dynamic session experiments. The grey bars represent baseline measurements without the exosuit, the blue bars represent measurements with the exosuit turned off, and the red bars represent measurements with active exosuit assistance. Brackets between conditions indicate significant differences. For muscle activation panels (a), (b), abbreviations denote specific muscles: deltoid (anterior, middle, posterior) as DELT (A, M, P), infraspinatus as INFRA, brachioradialis as BRACH, biceps as BIC, triceps as TRIC, extensor carpi ulnaris as ECU, and flexor carpi ulnaris as FCU.

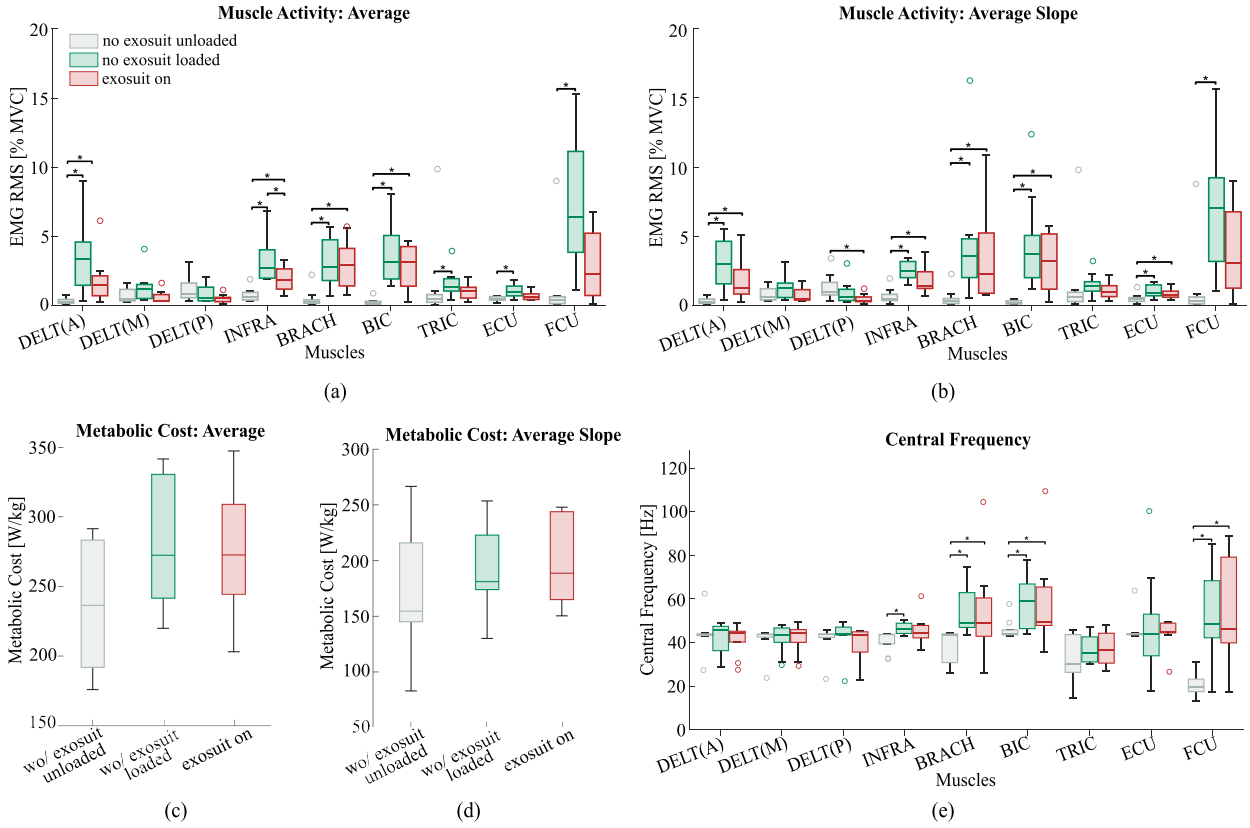

Fig. 8. Comparison of (a) average muscle activation, (b) average slope of muscle activity, (c) average metabolic cost, (d) average slope of metabolic cost, and (e) central frequency of muscle activation across three experimental conditions during endurance session experiments. Grey bars represent baseline measurements of walking without the exosuit and without load, green bars represent measurements of walking without the exosuit while carrying the load, and red bars represent measurements with active exosuit assistance while walking with the load. Brackets between conditions indicate significant differences. For muscle activation panels (a), (b), (e), abbreviations denote specific muscles: deltoid (anterior, middle, posterior) as DELT (A, M, P), infraspinatus as INFRA, brachioradialis as BRACH, biceps as BIC, triceps as TRIC, extensor carpi ulnaris as ECU, and flexor carpi ulnaris as FCU.

exosuit assistance, demonstrating comparable fatigue levels to the unloaded no-assistance condition.

C. User Perception

The SUS scores averaged 74.75 for both dynamic (range: 57.5–82.5) and endurance (range: 62.5–80) experiments, indicating that participants generally found the exosuit usable and acceptable for both tasks, as shown in Fig. 9(c). The spider plot in Fig. 9(d) illustrates user perceptions across usability dimensions, such as satisfaction, ease of use, functionality integration, and learnability, allowing a detailed comparison between dynamic and endurance experiments.

In dynamic experiments [see Fig. 9(b)], the perceived workload did not differ significantly between conditions. However, during endurance experiments [see Fig. 9(a)], the perceived physical demand and effort of unassisted loaded walking were significantly higher than those of unloaded walking ($P < 0.01$). Participants also rated physical demand significantly lower with exosuit assistance compared to unassisted loaded walking ($P < 0.05$), highlighting the perceived relief provided by the exosuit. In addition, perceived performance was significantly lower for unassisted loaded walking compared to unloaded walking ($P < 0.05$).

V. Discussion

This study evaluated the biomechanical and ergonomic performance of a hybrid soft-rigid elbow exosuit during dynamic and endurance tasks, revealing important insights and design implications.

While there are only a few works on the measurement of cuff pressure in exosuits [85], [86], [87], [88], the pressure measurement procedure in our study closely follows the methodology of a similar exosuit [85]. We showed that the pressure exerted by the exosuit cuffs on participants' skin was significantly below the thresholds reported in that comparable study, indicating enhanced comfort. This study tested varying levels of assistance, measuring the corresponding pressures up to 3-kg assistance.

The required assistance level depends on the specific application. For load-carrying tasks, maximum assistance may be necessary to minimize long-term muscle effort, which may come at the cost of increased discomfort. Conversely, clinical applications, such as post-stroke rehabilitation may require lower assistance to maximize comfort, ranging from 0.5 kg for patients with higher residual motor capabilities to 1.5–2.0 kg for fully supporting a flaccid elbow, typically corresponding to 2–2.5% of body weight.

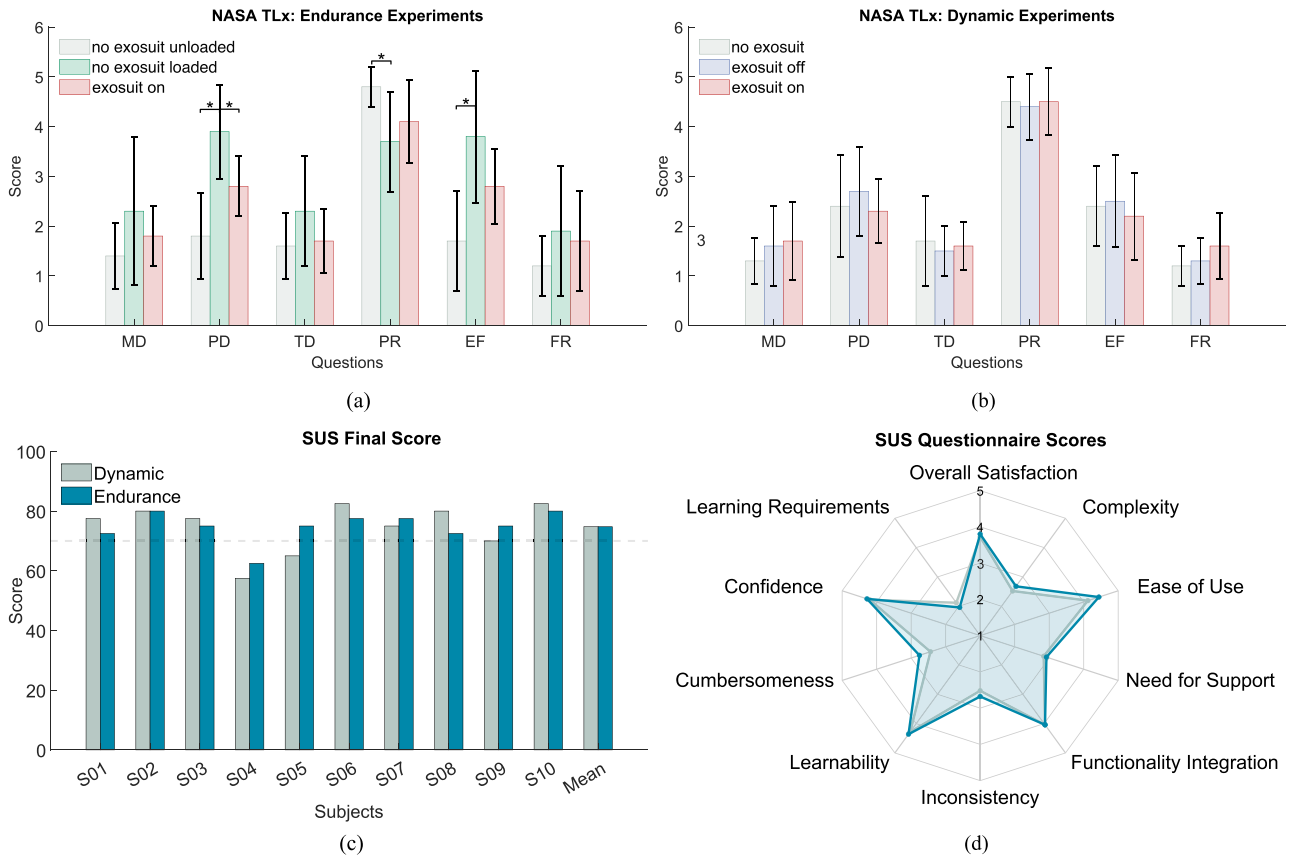

Fig. 9. Usability and NASA-Task Load Index questionnaire results. (a) NASA-TLX scores for the endurance session experiments across different experimental conditions. (b) NASA-TLX scores for the dynamic session experiments across different experimental conditions. (c) SUS scores for each participant, along with the mean score across participants in both endurance and dynamic experiments. (d) Average scores for each SUS question, comparing responses from participants in the dynamic and endurance sessions.

In most cases, measured pressures remained below 20 kPa, considered a discomfort threshold in literature [89], [90], validating the feasibility of the proposed design. As shown in the boxplots in Fig. 6, pressures were generally higher on the forearm cuffs compared to the upper arm cuffs, which can be attributed to the fact that the forearm cuffs directly bear the pulling forces generated by the actuation cables, while the upper arm cuffs primarily serve as cable routing points, and thus experience much lower direct forces. In addition, the variability in pressure values increased with higher assistance levels, reflecting the limitations of a one-size-fits-all design that may not accommodate all anthropometric variations. These findings highlight the importance of optimizing attachment strategies to balance comfort and functionality across diverse user groups.

While it may be intuitive to expect that only the lower side of the cuff would experience increased pressure with higher assistance, our results showed a moderate pressure rise on the upper side as well. This is explained by the geometry of the cable routing: the assistive force is applied at an angle, introducing not only an upward force but also a lateral component that generates shear forces and a bending moment on the cuff. This moment causes the cuff to press against the upper part of the arm, leading to a measurable pressure increase even on the upside of the cuff.

The ROM and bandwidth of the exosuit were sufficient to meet the functional requirements of average daily tasks [65], [91]. Although wearing the exosuit resulted in some reduction in ROM, participants were able to maintain a large ROM compared to the no-exosuit condition, as shown in Table IV. This ROM remained within the functional limits required to perform everyday tasks. In addition, the measured bandwidth represents a notable improvement over previously reported soft elbow exosuits [26] under comparable experimental conditions. These experimental results validate the design framework by demonstrating the exosuit's ability to accommodate user dynamics effectively.

From the smoothness and acceleration graphs in Fig. 7, it can be observed that acceleration was consistently lower in the exosuit-on condition, likely due to participants' lack of familiarity with the device, leading to smoother and less abrupt movements. This effect was more pronounced in proximal segments than in distal ones. In addition, the P, L, & P task showed a lower SPARC value for the forearm, accompanied by a higher SPARC value for the shoulder. This pattern may reflect a redistribution of movement effort: when the exosuit supported the forearm, participants had more shoulder motion to complete the task, which became less smooth compared to the unloaded condition.

The SUS results, depicted in Fig. 9(d), highlighted a low learning requirement and a moderate need for support among

participants, consistent with the exosuit's robust mechanical design and the objective of a generic controller. By eliminating the need for user-specific tuning, the system prioritized intuitive operation and rapid deployment in practical settings. This generic control approach, however, involves a tradeoff between simplicity and individual performance optimization. While the biceps, as the primary target muscle, consistently benefited from the assistance, intersubject differences in muscle activation suggest that a degree of personalization could further enhance performance. Future developments could incorporate human-in-the-loop (HIL) optimization strategies [92], [93], which automatically adjust control parameters to each user's biomechanics without requiring extensive calibration. Such methods have shown success in lower limb exosuits [94], [95] and represent a promising direction to balance plug-and-play usability with individualized adaptation in upper limb assistance.

The observed reductions in ROM during dynamic tasks with the exosuit, compared to the no-exosuit condition, were attributed to the braces worn by participants, which naturally limit movement. Notably, similar reductions in ROM were observed when the exosuit was powered OFF, and no significant differences were found between the powered-OFFand powered-ON conditions. These results confirm that the assistive forces provided by the exosuit did not restrict ROM during dynamic tasks. Furthermore, in the dynamic tasks, the active exosuit demonstrated assistance to the muscles without requiring higher muscle activity compared to the no-exosuit condition. Similarly, the powered-OFFexosuit did not lead to any significant change in muscle activity compared to the no-exosuit condition, except for the middle deltoid during the P, L, & P task. These findings, together with the ROM experiments and the ROM measurements during dynamic sessions, collectively demonstrate the kinematic and dynamic transparency of the exosuit during functional tasks.

The observed reductions in muscle activity are consistent with previously reported findings for cable-driven soft elbow exosuits. Prior studies demonstrated decreased activation of the biceps and delayed onset of fatigue in healthy participants assisted by similar devices [26], [39], [40]. While the exact magnitude of reduction varies across studies due to differences in tasks and assistance levels, our findings fall within the same range, confirming the efficacy of the proposed hybrid design in reducing user effort.

Although no significant improvements in metabolic cost were observed, participants reported a lower perceived physical demand when using the exosuit. This divergence between objective and subjective outcomes may stem from the relatively low intensity of the endurance task: metabolic cost reflects cumulative fatigue over time, whereas perceived effort captures immediate, qualitative sensations. Future studies could amplify task demands or personalize load carriage to better uncover metabolic benefits. In addition, the narrow treadmill used in this study likely contributed to the low walking speed, as participants expressed concerns about maintaining balance and safety while walking at higher speeds with a load. Addressing these limitations will enhance the reliability of future endurance assessments. Notably, with the exosuit activated, all the subjective perceptions appear positive with a notable difference with the without-exosuit loaded condition: this is more evident in the endurance evaluation rather than the dynamic one, given the challenging modality of the former.

It is also worth noting that the metabolic cost measured during the endurance task did not significantly differ between the assisted condition and the unassisted conditions, both with and without load. This suggests that the exosuit was able to offset the energetic penalty typically associated with device weight, effectively neutralizing its metabolic impact. Despite the system weighing approximately 4 kg, it did not increase user effort during walking. This finding supports the practical benefit of the exosuit in its current form. However, we acknowledge that the device is yet to be optimized for weight. Future designs will target a total weight closer to 2 kg, primarily through back unit and battery integration improvements, to enhance comfort and further improve energy efficiency.

The exosuit's assistance provided significant benefits for the infraspinatus and middle deltoid muscles, which are essential for shoulder stabilization and load carrying [96]. This reduction can be explained by the mechanical coupling within the upper limb: when the forearm is supported, the shoulder no longer needs to generate as much stabilizing torque to compensate for the forearm's weight and dynamics. This interpretation aligns with simulation-based studies [97], [98], which have shown that assisting a single joint can alter muscle demands at adjacent joints. While these simulations provide important insights, related biomechanical studies have also reported reduced shoulder muscle activity when static forearm support is provided [99], [100], [101]. Although these studies did not use exosuits, they highlight the same underlying principle: supporting the forearm can indirectly reduce shoulder muscle activity. In addition, the absence of significant activity increases in the triceps and wrist flexor/extensor muscles suggests that the assistance did not impose compensatory demands elsewhere.

These findings demonstrate that analyzing the entire upper limb, rather than focusing solely on the assisted joint, is crucial for understanding how exosuit assistance affects human biomechanics. Full-arm kinematics and biomechanics data revealed how users adapt their movement strategies, including compensations or redistribution of effort across other joints. Our experimental design enabled us to capture this broader perspective, showing that assistive forces applied at the elbow can influence shoulder and wrist motion as well.

VI. Conclusion

This study introduced and evaluated a hybrid soft-rigid elbow exosuit designed to assist the elbow joint, focusing on its ergonomics, usability, and biomechanical impacts during dynamic and endurance tasks. A lumped-parameter internal dynamics model of the exosuit was developed, providing critical design guidelines to optimize assistive force delivery, system efficiency, and wearer comfort. These insights led to the development of a robust hybrid exosuit that combines high efficiency, improved bandwidth, and better force distribution, meeting the demands of both performance and usability.

The results confirmed key design objectives, such as high bandwidth, ensuring rapid and smooth assistance across various tasks. The double-cable architecture effectively distributed forces, reducing localized pressure on the wearer's limb and enhancing comfort. ROM experiments demonstrated that the exosuit does not obstruct daily activities, further underscoring its ergonomic design.

The biomechanical impact of the exosuit was assessed through dynamic and endurance tasks. To enable a more realistic evaluation of the exosuit for clinical and everyday use by nontechnical users, a generic interaction control setting and fixed geometric and gravity assistance parameters were employed throughout the experiments without personalization. During dynamic tasks, the exosuit significantly reduced biceps muscle activity compared to unassisted conditions, while in endurance tasks, it effectively reduced infraspinatus activation and mitigated load increases across other muscles. Subjective assessments indicated a perceived reduction in physical demand during endurance sessions and usability of the device, highlighting the intuitive and supportive nature of the system.

This study emphasizes the importance of integrating robust mechatronic design with a high-performance generic controller to deliver effective assistance across diverse users without extensive customization. However, the results also revealed meaningful intersubject variability in outcomes, emphasizing the tradeoff of using a generic controller. Future work will focus on addressing this tradeoff by developing strategies for personalizing the controller that do not require user involvement or technical tuning, ensuring the exosuit remains practical and user-friendly in both clinical and real-world applications. In addition, efforts will focus on improving wearability and expanding evaluations to include broader tasks and clinical applications, particularly in rehabilitation and load-carrying scenarios.

APPENDIX

$$G(s) = \frac{N(s)}{D(s)} \tag{A1}$$

$$N(s) = k_c\, k_t + b_c\, k_t\, s + b_t\, k_c\, s + b_c\, b_t\, s^2 \tag{A2}$$

$$D(s) = \alpha_6\, s^6 + \alpha_5\, s^5 + \alpha_4\, s^4 + \alpha_3\, s^3 + \alpha_2\, s^2 + \alpha_1\, s + \alpha_0 \tag{A3}$$

$$\alpha_6 = m_c\, m_h\, m_m$$

$$\alpha_5 = b_c\, m_c\, m_m + b_c\, m_h\, m_m + b_h\, m_c\, m_m + b_m\, m_c\, m_h + b_t\, m_c\, m_h + b_t\, m_h\, m_m$$

$$\alpha_4 = b_c\, b_m\, m_c + b_c\, b_h\, m_m + b_c\, b_m\, m_h + b_h\, b_m\, m_c + b_c\, b_t\, m_c + b_c\, b_t\, m_h + b_h\, b_t\, m_c + b_c\, b_t\, m_m + b_h\, b_t\, m_m + b_m\, b_t\, m_h + k_c\, m_c\, m_m + k_c\, m_h\, m_m + k_h\, m_c\, m_m + k_t\, m_c\, m_h + k_t\, m_h\, m_m$$

$$\alpha_3 = b_c\, b_h\, b_m + b_c\, b_h\, b_t + b_c\, b_m\, b_t + b_h\, b_m\, b_t + b_m\, k_c\, m_c + b_c\, k_h\, m_m + b_h\, k_c\, m_m + b_m\, k_c\, m_h + b_m\, k_h\, m_c + b_c\, k_t\, m_c + b_t\, k_c\, m_c + b_c\, k_t\, m_h + b_h\, k_t\, m_c + b_t\, k_c\, m_h + b_t\, k_h\, m_c + b_c\, k_t\, m_m + b_t\, k_c\, m_m + b_h\, k_t\, m_m + b_m\, k_t\, m_h + b_t\, k_h\, m_m$$

$$\alpha_2 = b_c\, b_m\, k_h + b_h\, b_m\, k_c + b_c\, b_h\, k_t + b_c\, b_t\, k_h + b_h\, b_t\, k_c + b_c\, b_m\, k_t + b_m\, b_t\, k_c + b_h\, b_m\, k_t + b_m\, b_t\, k_h + k_c\, k_h\, m_m + k_c\, k_t\, m_c + k_c\, k_t\, m_h + k_h\, k_t\, m_c + k_c\, k_t\, m_m + k_h\, k_t\, m_m$$

$$\alpha_1 = b_m\, k_c\, k_h + b_c\, k_h\, k_t + b_h\, k_c\, k_t + b_t\, k_c\, k_h + b_m\, k_c\, k_t + b_m\, k_h\, k_t$$

$$\alpha_0 = k_c\, k_h\, k_t.$$

ACKNOWLEDGMENT

The authors would like to sincerely thank all participants for their time and contributions during the experimental evaluation.

REFERENCES

[1] T. Proietti, E. Ambrosini, A. Pedrocchi, and S. Micera, "Wearable robotics for impaired upper-limb assistance and rehabilitation: State of the art and future perspectives," *IEEE Access*, vol. 10, pp. 106117–106134, 2022.

[2] G. S. Sawicki, O. N. Beck, I. Kang, and A. J. Young, "The exoskeleton expansion: Improving walking and running economy," *J. Neuroengineering Rehabil.*, vol. 17, 2020, Art. no. 25.

[3] C. Siviy et al., "Opportunities and challenges in the development of exoskeletons for locomotor assistance," *Nature Biomed. Eng.*, vol. 7, no. 4, pp. 456–472, 2023.

[4] T. Moeller, J. Krell-Roesch, A. Woll, and T. Stein, "Effects of upper-limb exoskeletons designed for use in the working environment—A literature review," *Front. Robot. AI*, vol. 9, 2022, Art. no. 858893.

[5] M. P. De Looze, T. Bosch, F. Krause, K. S. Stadler, and L. W. O'sullivan, "Exoskeletons for industrial application and their potential effects on physical work load," *Ergonomics*, vol. 59, no. 5, pp. 671–681, 2016.

[6] M. Xiloyannis et al., "Soft robotic suits: State of the art, core technologies, and open challenges," *IEEE Trans. Robot.*, vol. 38, no. 3, pp. 1343–1362, Jun. 2022.

[7] A. J. Young and D. P. Ferris, "State of the art and future directions for lower limb robotic exoskeletons," *IEEE Trans. Neural Syst. Rehabil. Eng.*, vol. 25, no. 2, pp. 171–182, Feb. 2017.

[8] S. Crea et al., "Occupational exoskeletons: A roadmap toward large-scale adoption. methodology and challenges of bringing exoskeletons to workplaces," *Wearable Technol.*, vol. 2, 2021, Art. no. e11.

[9] T.-W. P. Huang and A. D. Kuo, "Mechanics and energetics of load carriage during human walking," *J. Exp. Biol.*, vol. 217, no. 4, pp. 605–613, 2014.

[10] R. C. Browning, E. A. Baker, J. A. Herron, and R. Kram, "Effects of obesity and sex on the energetic cost and preferred speed of walking," *J. Appl. Physiol.*, vol. 100, no. 2, pp. 390–398, 2006.

[11] N. Jarrassé and G. Morel, "Connecting a human limb to an exoskeleton," *IEEE Trans. Robot.*, vol. 28, no. 3, pp. 697–709, Jun. 2012.

[12] R. Mallat, M. Khalil, G. Venture, V. Bonnet, and S. Mohammed, "Human-exoskeleton joint misalignment: A systematic review," in *Proc. IEEE 5th Int. Conf. Adv. Biomed. Eng.*, 2019, pp. 1–4.

[13] A. T. Asbeck, S. M. De Rossi, I. Galiana, Y. Ding, and C. J. Walsh, "Stronger, smarter, softer: Next-generation wearable robots," *IEEE Robot. Automat. Mag.*, vol. 21, no. 4, pp. 22–33, Dec. 2014.

[14] J. L. Pons, "Witnessing a wearables transition," *Science*, vol. 365, no. 6454, pp. 636–637, 2019.

[15] E. Martini et al., "Gait training using a robotic hip exoskeleton improves metabolic gait efficiency in the elderly," *Sci. Rep.*, vol. 9, no. 1, 2019, Art. no. 7157.

[16] K. A. Witte, P. Fiers, A. L. Sheets-Singer, and S. H. Collins, "Improving the energy economy of human running with powered and unpowered ankle exoskeleton assistance," *Sci. Robot.*, vol. 5, no. 40, 2020, Art. no. eaay9108.

[17] J. Park et al., "Effect of hip abduction assistance on metabolic cost and balance during human walking," *Sci. Robot.*, vol. 8, no. 83, 2023, Art. no. eade0876.

[18] X. Zhang et al., "A lower limb wearable exosuit for improved sitting, standing, and walking efficiency," *IEEE Trans. Robot.*, vol. 41, pp. 127–140, 2025.

[19] K. Swaminathan et al., "Ankle-targeted exosuit resistance increases paretic propulsion in people post-stroke," *J. NeuroEngineering Rehabil.*, vol. 20, no. 1, Art. no. 85, Jun. 2023.

[20] S. Sridar, Z. Qiao, N. Muthukrishnan, W. Zhang, and P. Polygerinos, "A soft-inflatable exosuit for knee rehabilitation: Assisting swing phase during walking," *Front. Robot. AI*, vol. 5, 2018, Art. no. 44.

[21] J. Kim et al., "Soft robotic apparel to avert freezing of gait in Parkinson's disease," *Nature Med.*, vol. 30, no. 1, pp. 177–185, Jan. 2024.

[22] Y. M. Zhou et al., "A portable inflatable soft wearable robot to assist the shoulder during industrial work," *Sci. Robot.*, vol. 9, no. 91, 2024, Art. no. eadi2377.

[23] Y. G. Kim, M. Xiloyannis, D. Accoto, and L. Masia, "Development of a soft exosuit for industrial applications," in *Proc. 7th IEEE Int. Conf. Biomed. Robot. Biomechatronics*, 2018, pp. 324–329.

[24] J. Chung et al., "Lightweight active back exosuit reduces muscular effort during an hour-long order picking task," *Commun. Eng.*, vol. 3, no. 1, 2024, Art. no. 35.

[25] E. Mobedi, W. Kim, M. Leonori, N. G. Tsagarakis, and A. Ajoudani, "Design and control of an assistive device for elbow effort-compensation," *IEEE/ASME Trans. Mechatron.*, vol. 28, no. 6, pp. 3446–3457, Dec. 2023.

[26] M. Xiloyannis, D. Chiaradia, A. Frisoli, and L. Masia, "Physiological and kinematic effects of a soft exosuit on arm movements," *J. Neuroengineering Rehabil.*, vol. 16, 2019, Art. no. 29.

[27] A.-M. Georgarakis, M. Xiloyannis, P. Wolf, and R. Riener, "A textile exomuscle that assists the shoulder during functional movements for everyday life," *Nature Mach. Intell.*, vol. 4, no. 6, pp. 574–582, 2022.

[28] T. Proietti et al., "Restoring arm function with a soft robotic wearable for individuals with amyotrophic lateral sclerosis," *Sci. Transl. Med.*, vol. 15, no. 681, Art. no. eadd1504, 2023.

[29] N. Lotti et al., "Soft robotics to enhance upper limb endurance in individuals with multiple sclerosis," *Soft Robot.*, vol. 11, no. 2, pp. 338–346, 2024.

[30] C. Nam et al., "An exoneuromusculoskeleton for self-help upper limb rehabilitation after stroke," *Soft Robot.*, vol. 9, no. 1, pp. 14–35, 2022.

[31] C. Simpson, B. Huerta, S. Sketch, M. Lansberg, E. Hawkes, and A. Okamura, "Upper extremity exomuscle for shoulder abduction support," *IEEE Trans. Med. Robot. Bionics*, vol. 2, no. 3, pp. 474–484, Aug. 2020.

[32] C. O'Neill et al., "Inflatable soft wearable robot for reducing therapist fatigue during upper extremity rehabilitation in severe stroke," *IEEE Robot. Automat. Lett.*, vol. 5, no. 3, pp. 3899–3906, Jul. 2020.

[33] N. P. Fromme et al., "Development of a textile integrated, two-state controlled tremor suppression orthosis for the wrist," *IEEE Trans. Med. Robot. Bionics*, vol. 5, no. 3, pp. 683–703, Aug. 2023.

[34] E. Bardi, M. Gandolla, F. Braghin, F. Resta, A. L. Pedrocchi, and E. Ambrosini, "Upper limb soft robotic wearable devices: A systematic review," *J. NeuroEngineering Rehabil.*, vol. 19, no. 1, 2022, Art. no. 87.

[35] C. Thalman and P. Artemiadis, "A review of soft wearable robots that provide active assistance: Trends, common actuation methods, fabrication, and applications," *Wearable Technol.*, vol. 1, 2020, Art. no. e3.

[36] S. Hussain and F. Ficuciello, "Advancements in soft wearable robots: A systematic review of actuation mechanisms and physical interfaces," *IEEE Trans. Med. Robot. Bionics*, vol. 6, no. 3, pp. 903–929, 2024.

[37] I. Koo et al., "Development of a meal assistive exoskeleton made of soft materials for polymyositis patients," in *Proc. IEEE/RSJ Int. Conf. Intell. Robots Syst.*, 2014, pp. 542–547.

[38] C. J. Nycz, M. A. Delph, and G. S. Fischer, "Modeling and design of a tendon actuated soft robotic exoskeleton for hemiparetic upper limb rehabilitation," in *Proc. 37th Annu. Int. Conf. IEEE Eng. Med. Biol. Soc.*, 2015, pp. 3889–3892.

[39] D. Chiaradia, M. Xiloyannis, C. W. Antuvan, A. Frisoli, and L. Masia, "Design and embedded control of a soft elbow exosuit," in *Proc. IEEE Int. Conf. Soft Robot.*, 2018, pp. 565–571.

[40] F. Missiroli et al., "Rigid, soft, passive, and active: A hybrid occupational exoskeleton for bimanual multijoint assistance," *IEEE Robot. Automat. Lett.*, vol. 7, no. 2, pp. 2557–2564, Apr. 2022.

[41] B. Noronha et al., "Soft, lightweight wearable robots to support the upper limb in activities of daily living: A feasibility study on chronic stroke patients," *IEEE Trans. Neural Syst. Rehabil. Eng.*, vol. 30, pp. 1401–1411, 2022.

[42] M. Xiloyannis, "Development and validation of a soft robotic exosuit for assistance of the upper limbs," Ph.D. dissertation, Interdisciplinary Graduate School, NTU Institute for Health Technologies, Nanyang Technological University, Singapore, 2019.

[43] C. M. Harbauer, M. Fleischer, T. Nguyen, F. Bos, and K. Bengler, "Too close to comfort? a new approach of designing a soft cable-driven exoskeleton for lifting tasks under ergonomic aspects," in *Proc. 3rd Int. Conf. Intell. Robotic Control Eng.*, 2020, pp. 105–109.

[44] N. Li et al., "Bio-inspired upper limb soft exoskeleton to reduce stroke-induced complications," *Bioinspiration Biomimetics*, vol. 13, no. 6, 2018, Art. no. 066001.

[45] J. L. Samper-Escudero, A. Gimenez-Fernandez, M. Á. Sánchez-Urán, and M. Ferre, "A cable-driven exosuit for upper limb flexion based on fibres compliance," *IEEE Access*, vol. 8, pp. 153297–153310, 2020.

[46] Q. Wu, B. Chen, and H. Wu, "Neural-network-enhanced torque estimation control of a soft wearable exoskeleton for elbow assistance," *Mechatronics*, vol. 63, 2019, Art. no. 102279.

[47] G. Palli and C. Melchiorri, "Model and control of tendon-sheath transmission systems," in *Proc. IEEE Int. Conf. Robot. Automat.*, 2006, pp. 988–993.

[48] D. Chen, Y. Yun, and A. D. Deshpande, "Experimental characterization of Bowden cable friction," in *Proc. IEEE Int. Conf. Robot. Automat.*, 2014, pp. 5927–5933.

[49] M. Kaneko, W. Paetsch, and H. Tolle, "Input-dependent stability of joint torque control of tendon-driven robot hands," *IEEE Trans. Ind. Electron.*, vol. 39, no. 2, pp. 96–104, Apr. 1992.

[50] B. K. Dinh, M. Xiloyannis, L. Cappello, C. W. Antuvan, S.-C. Yen, and L. Masia, "Adaptive backlash compensation in upper limb soft wearable exoskeletons," *Robot. Auton. Syst.*, vol. 92, pp. 173–186, 2017.

[51] A. Schiele, P. Letier, R. Van Der Linde, and F. Van Der Helm, "Bowden cable actuator for force-feedback exoskeletons," in *Proc. IEEE/RSJ Int. Conf. Intell. Robots Syst.*, 2006, pp. 3599–3604.

[52] S. Eppinger and W. Seering, "Understanding bandwidth limitations in robot force control," in *Proc. IEEE Int. Conf. Robot. Automat.*, 1987, pp. 904–909.

[53] E. Colgate and N. Hogan, "An analysis of contact instability in terms of passive physical equivalents," in *Proc. IEEE Int. Conf. Robot. Automat.*, 1989, pp. 404–409.

[54] A. Q. Keemink, H. Van der Kooij, and A. H. Stienen, "Admittance control for physical human–robot interaction," *Int. J. Robot. Res.*, vol. 37, no. 11, pp. 1421–1444, 2018.

[55] A. T. Asbeck, S. M. De Rossi, K. G. Holt, and C. J. Walsh, "A biologically inspired soft exosuit for walking assistance," *Int. J. Robot. Res.*, vol. 34, no. 6, pp. 744–762, 2015.

[56] M. B. Yandell, B. T. Quinlivan, D. Popov, C. Walsh, and K. E. Zelik, "Physical interface dynamics alter how robotic exosuits augment human movement: Implications for optimizing wearable assistive devices," *J. Neuroengineering Rehabil.*, vol. 14, 2017, Art. no. 40.

[57] J. Cool, "Biomechanics of orthoses for the subluxed shoulder," *Prosthetics Orthotics Int.*, vol. 13, no. 2, pp. 90–96, 1989.

[58] M. Zhang and V. Roberts, "The effect of shear forces externally applied to skin surface on underlying tissues," *J. Biomed. Eng.*, vol. 15, no. 6, pp. 451–456, 1993.

[59] H. Choi, B. B. Kang, B.-K. Jung, and K.-J. Cho, "Exo-wrist: A soft tendon-driven wrist-wearable robot with active anchor for dart-throwing motion in hemiplegic patients," *IEEE Robot. Automat. Lett.*, vol. 4, no. 4, pp. 4499–4506, Oct. 2019.

[60] K. Witherspoon and A. Kernbaum, "Flexgrip," U.S. Patent Appl. 20180049903A1, 2018.

[61] M. Bottlang, S. Madey, C. Steyers, J. Marsh, and T. Brown, "Assessment of elbow joint kinematics in passive motion by electromagnetic motion tracking," *J. Orthopaedic Res.*, vol. 18, no. 2, pp. 195–202, 2000.

[62] T. R. Duck, C. E. Dunning, G. J. King, and J. A. Johnson, "Variability and repeatability of the flexion axis at the ulnohumeral joint," *J. Orthopaedic Res.*, vol. 21, no. 3, pp. 399–404, 2003.

[63] A. Ericson, A. Arndt, A. Stark, P. Wretenberg, and A. Lundberg, "Variation in the position and orientation of the elbow flexion axis," *J. Bone Joint Surg. Brit.*, vol. 85, no. 4, pp. 538–544, 2003.

[64] B. Morrey, L. Askew, and E. Chao, "A biomechanical study of normal functional elbow motion," *JBJS*, vol. 63, no. 6, pp. 872–877, 1981.

[65] M. Buckley, A. Yardley, G. Johnson, and D. Cams, "Dynamics of the upper limb during performance of the tasks of everyday living—A review of the current knowledge base," *Proc. Inst. Mech. Eng., Part H: J. Eng. Med.*, vol. 210, no. 4, pp. 241–247, 1996.

[66] J. Loftice, G. S. Fleisig, N. Zheng, and J. R. Andrews, "Biomechanics of the elbow in sports," *Clin. Sports Med.*, vol. 23, no. 4, pp. 519–530, 2004.

[67] I. A. Murray and G. R. Johnson, "A study of the external forces and moments at the shoulder and elbow while performing every day tasks," *Clin. Biomech.*, vol. 19, no. 6, pp. 586–594, 2004.
[68] Y. Jung and J. Bae, "Torque control of a series elastic tendon-sheath actuation mechanism," *IEEE/ASME Trans. Mechatron.*, vol. 25, no. 6, pp. 2915–2926, Dec. 2020.
[69] Q. Wu, X. Wang, L. Chen, and F. Du, "Transmission model and compensation control of double-tendon-sheath actuation system," *IEEE Trans. Ind. Electron.*, vol. 62, no. 3, pp. 1599–1609, Mar. 2015.
[70] T. Do, T. Tjahjowidodo, M. Lau, and S. Phee, "Nonlinear friction modelling and compensation control of hysteresis phenomena for a pair of tendon-sheath actuated surgical robots," *Mech. Syst. Signal Process.*, vol. 60, pp. 770–784, 2015.
[71] Y. Shi et al., "Human-in-the-loop modeling and control of an upper limb exosuit with tendon-sheath actuation," *IEEE Robot. Automat. Lett.*, vol. 9, no. 6, pp. 5919–5926, Jun. 2024.
[72] G. Palli, G. Borghesan, and C. Melchiorri, "Modeling, identification, and control of tendon-based actuation systems," *IEEE Trans. Robot.*, vol. 28, no. 2, pp. 277–290, Apr. 2011.
[73] M. Kaneko, M. Wada, H. Maekawa, and K. Tanie, "A new consideration on tendon-tension control system of robot hands," in *Proc. IEEE Int. Conf. Robot. Automat.*, 1991, pp. 1028–1029.
[74] R. S. Razavian, M. Sadeghi, S. Bazzi, R. Nayeem, and D. Sternad, "Body mechanics, optimality, and sensory feedback in the human control of complex objects," *Neural Computation*, vol. 35, no. 5, pp. 853–895, 2023.
[75] S. Bazzi, S. Stansfield, N. Hogan, and D. Sternad, "Simplified internal models in human control of complex objects," *PLOS Comput. Biol.*, vol. 20, no. 11, 2024, Art. no. e1012599.
[76] W. Townsend and J. Salisbury, "The effect of Coulomb friction and stiction on force control," in *Proc. IEEE Int. Conf. Robot. Automat.*, 1987, pp. 883–889.
[77] A. Calanca, R. Muradore, and P. Fiorini, "A review of algorithms for compliant control of stiff and fixed-compliance robots," *IEEE/ASME Trans. Mechatron.*, vol. 21, no. 2, pp. 613–624, Apr. 2016.
[78] D. Chiaradia, L. Tiseni, M. Xiloyannis, M. Solazzi, L. Masia, and A. Frisoli, "An assistive soft wrist exosuit for flexion movements with an ergonomic reinforced glove," *Front. Robot. AI*, vol. 7, 2021, Art. no. 595862.
[79] W. Yu, J. Rosen, and X. Li, "PID admittance control for an upper limb exoskeleton," in *Proc. Amer. Control Conf.*, 2011, pp. 1124–1129.
[80] E. Criswell, *Cram's Introduction to Surface Electromyography*. Boston, MA, USA: Jones & Bartlett Learn., 2010.
[81] J. Brockway, "Derivation of formulae used to calculate energy expenditure in man," *Hum. Nutr. Clin. Nutr.*, vol. 41, no. 6, pp. 463–471, 1987.
[82] J. Brooke, "SUS: A quick and dirty usability scale," in *Usability Evaluation in Industry*. Boca Raton, FL, USA: CRC Press, 1996.
[83] S. Balasubramanian, A. Melendez-Calderon, A. Roby-Brami, and E. Burdet, "On the analysis of movement smoothness," *J. Neuroengineering Rehabil.*, vol. 12, 2015, Art. no. 112.
[84] M. Schimpl et al., "Association between walking speed and age in healthy, free-living individuals using mobile accelerometry—A cross-sectional study," *PLoS One*, vol. 6, no. 8, 2011, Art. no. e23299.
[85] M. Xiloyannis, D. Chiaradia, A. Frisoli, and L. Masia, "Characterisation of pressure distribution at the interface of a soft exosuit: Towards a more comfortable wear," in *Proc. Wearable Robot.: Challenges Trends: Proc. 4th Int. Symp. Wearable Robot.*, 2019, pp. 35–38.
[86] A.-M. Georgarakis, R. Stämpfli, P. Wolf, R. Riener, and J. E. Duarte, "A method for quantifying interaction forces in wearable robots," in *Proc. 7th IEEE Int. Conf. Biomed. Robot. Biomechatronics*, 2018, pp. 789–794.
[87] B. Quinlivan, A. Asbeck, D. Wagner, T. Ranzani, S. Russo, and C. Walsh, "Force transfer characterization of a soft exosuit for gait assistance," in *Proc. Int. Des. Eng. Tech. Conf. Comput. Inf. Eng. Conf.*, 2015, Art. no. V05AT08A049.
[88] S. Massardi, D. Rodriguez-Cianca, D. Pinto-Fernandez, J. C. Moreno, M. Lancini, and D. Torricelli, "Characterization and evaluation of human–exoskeleton interaction dynamics: A review," *Sensors*, vol. 22, no. 11, 2022, Art. no. 3993.
[89] T. Kermavnar, V. Power, A. de Eyto, and L. W. O'Sullivan, "Computerized cuff pressure algometry as guidance for circumferential tissue compression for wearable soft robotic applications: A systematic review," *Soft Robot.*, vol. 5, no. 1, pp. 1–16, 2018.
[90] T. Kermavnar, V. Power, A. de Eyto, and L. O'Sullivan, "Cuff pressure algometry in patients with chronic pain as guidance for circumferential tissue compression for wearable soft exoskeletons: A systematic review," *Soft Robot.*, vol. 5, no. 5, pp. 497–511, 2018.
[91] A. M. Oosterwijk, M. K. Nieuwenhuis, C. P. van der Schans, and L. J. Mouton, "Shoulder and elbow range of motion for the performance of activities of daily living: A systematic review," *Physiotherapy Theory Pract.*, vol. 34, no. 7, pp. 505–528, 2018.
[92] P. Slade et al., "On human-in-the-loop optimization of human–robot interaction," *Nature*, vol. 633, no. 8031, pp. 779–788, 2024.
[93] M. A. Diaz et al., "Human-in-the-loop optimization of wearable robotic devices to improve human–robot interaction: A systematic review," *IEEE Trans. Cybern.*, vol. 53, no. 12, pp. 7483–7496, Dec. 2022.
[94] Y. Ding, M. Kim, S. Kuindersma, and C. J. Walsh, "Human-in-the-loop optimization of hip assistance with a soft exosuit during walking," *Sci. Robot.*, vol. 3, no. 15, 2018, Art. no. eaar5438.
[95] J. Zhang et al., "Human-in-the-loop optimization of exoskeleton assistance during walking," *Science*, vol. 356, no. 6344, pp. 1280–1284, 2017.
[96] A. Song, N. Kuznetsov, S. Winges, and M. MacLellan, "Muscle synergy for upper limb damping behavior during object transport while walking in healthy young individuals," *Exp. Brain Res.*, vol. 238, pp. 1203–1218, 2020.
[97] A. KhalilianMotamed Bonab, D. Chiaradia, A. Frisoli, and D. Leonardis, "A framework for modeling, optimization, and musculoskeletal simulation of an elbow–wrist exosuit," *Robotics*, vol. 13, no. 4, 2024, Art. no. 60.
[98] C. L. Dembia, A. Silder, T. K. Uchida, J. L. Hicks, and S. L. Delp, "Simulating ideal assistive devices to reduce the metabolic cost of walking with heavy loads," *PLoS One*, vol. 12, no. 7, 2017, Art. no. e0180320.
[99] D. Odell, A. Barr, R. Goldberg, J. Chung, and D. Rempel, "Evaluation of a dynamic arm support for seated and standing tasks: A laboratory study of electromyography and subjective feedback," *Ergonomics*, vol. 50, no. 4, pp. 520–535, 2007.
[100] L. C. Onyebeke, J. G. Young, M. B. Trudeau, and J. T. Dennerlein, "Effects of forearm and palm supports on the upper extremity during computer mouse use," *Appl. Ergonom.*, vol. 45, no. 3, pp. 564–570, 2014.
[101] J. S. Gonçalves, C. S. Moriguchi, K. S. Takekawa, H. J. C. G. Coury, and T. de Oliveira Sato, "The effects of forearm support and shoulder posture on upper trapezius and anterior deltoid activity," *J. Phys. Ther. Sci.*, vol. 29, no. 5, pp. 793–798, 2017.

Ali KhalilianMotamed Bonab received the M.Sc. degree in mechatronics engineering from Sabanci University, Istanbul, Turkey, in 2021, and he is a Ph.D. candidate in the emerging digital technologies program, perceptual robotics curriculum, of the Institute of Mechanical Intelligence, Scuola Superiore Sant'Anna, Pisa, Italy.

He spent a visiting period as a Visiting Ph.D. Candidate with the Sensory-Motor Systems Laboratory, ETH Zurich, Zurich, Switzerland. His research interests include wearable robotics, assistive and rehabilitation robotics, physical human–robot interaction, musculoskeletal simulation, and haptic feedback systems.

Cristian Camardella received the master's degree in control theory and automation engineering from the Polytechnic of Bari, Bari, Italy, in 2017, and the Ph.D. degree in emerging digital technologies, perceptual robotics curriculum, from Scuola Superiore Sant'Anna, Pisa, Italy, in 2021.

He is currently a Researcher with the Perceptual Robotics Laboratory, Mechanical Intelligence Institute, Scuola Superiore Sant'Anna. He is currently working on distributed haptic systems, predictive systems, and robotic platforms in the rehabilitation robotics field, and immersive VR serious games. His research interests include machine learning and artificial intelligence, robotic exoskeletons and control strategies, muscle synergies, and serious game optimization.

Antonio Frisoli (Senior Member, IEEE) received the M.S. degree with honors in mechanical engineering from University of Pisa, Italy, in 1998, and the Ph.D. degree in industrial and computer science engineering from Scuola Superiore Sant'Anna, Pisa, Italy, in 2002. He is currently a Full Professor of Engineering Mechanics and Robotics with Scuola Superiore Sant'Anna (SSSA), Pisa, Italy, where he leads the Human–Robot Interaction, Intelligence Mechanical Institute, and is also currently responsible for the SSSA macro node of the Artes 4.0 competence center on collaborative robotics. He is very active in technology transfer and open innovation and has been the Co-Founder of two spin-offs (Wearable Robotics srl, Ghezzano, Italy, and Next Generation Robotics srl, Pisa, Italy). His research interests include the area of collaborative, rehabilitation, and wearable robotics, exoskeletons, multimodal interaction and haptics, wearable devices, and virtual reality.

Dr. Frisoli is an Associate Editor for *IEEE Robotics Automation Magazine* and covers several scientific and editorial roles in scientific societies (Eurohaptics and International Consortium for Rehabilitation Robotics), international conferences, and journals.

Domenico Chiaradia received the M.S. degree with honors in control theory and automation engineering from the Polytechnic University of Bari, Bari, Italy, in 2014, and the Ph.D. degree in emerging digital technologies, perceptual robotics curriculum, from Scuola Superiore Sant'Anna, Pisa, Italy, in 2018.

He is an Assistant Professor of Mechanical Engineering focusing on Robotics with Sant'Anna School of Advanced Studies, Pisa, Italy. He leads the group developing flexible and portable exoskeletons, and soft exosuits in the human robot interaction research area. His research interests include physical human–robot interaction, rigid and flexible exoskeletons and soft exosuits for assistance and rehabilitation, mechanical design and control of flexible joints, and haptic interfaces.

Open Access provided by 'Scuola Superiore "S.Anna" di Studi Universitari e di Perfezionamento 2025-2027 Deposit Account' within the CRUI CARE Agreement